*minerals*

MDPI

*Article*

# Mineral-Melt Equilibria and Geothermobarometry of Campi Flegrei Magmas: Inferences for Magma Storage Conditions

**Carlo Pelullo [1,2,*], Raffaella Silvia Iovine [2], Ilenia Arienzo [2], Valeria Di Renzo [1], Lucia Pappalardo [2], Paola Petrosino [1] and Massimo D'Antonio [1,*]**

[1] Dipartimento di Scienze della Terra, dell'Ambiente e delle Risorse, Università di Napoli Federico II, Monte Sant'Angelo, Via Vicinale Cupa Cintia, 21-80126 Napoli, Italy; valeria.direnzo@unina.it (V.D.R.); petrosin@unina.it (P.P.)

[2] Sezione di Napoli Osservatorio Vesuviano, Istituto Nazionale di Geofisica e Vulcanologia, Via Diocleziano, 328-80124 Napoli, Italy; raffaella.iovine@gmail.com (R.S.I.); ilenia.arienzo@ingv.it (I.A.); lucia.pappalardo@ingv.it (L.P.)

* Correspondence: carlo.pelullo@unina.it (C.P.); masdanto@unina.it (M.D.)

**Abstract:** The eruptions of Campi Flegrei (Southern Italy), one of the most studied and dangerous active volcanic areas of the world, are fed by mildly potassic alkaline magmas, from shoshonite to trachyte and phonotrachyte. Petrological investigations carried out in past decades on Campi Flegrei rocks provide crucial information for understanding differentiation processes in its magmatic system. However, the compositional features of rocks are a palimpsest of many processes acting over timescales of $10^0$–$10^4$ years, including crystal entrapment from multiple reservoirs with different magmatic histories. In this work, olivine, clinopyroxene and feldspar crystals from volcanic rocks related to the entire period of Campi Flegrei's volcanic activity are checked for equilibrium with combined and possibly more rigorous tests than those commonly used in previous works (e.g., Fe–Mg exchange between either olivine or clinopyroxene and melt), with the aim of obtaining more robust geothermobarometric estimations for the magmas these products represent. We applied several combinations of equilibrium tests and geothermometric and geobarometric methods to a suite of rocks and related minerals spanning the period from ~59 ka to 1538 A.D. and compared the obtained results with the inferred magma storage conditions estimated in previous works through different methods. This mineral-chemistry investigation suggests that two prevalent sets of T–P (temperature–pressure) conditions, here referred to as "magmatic environments", characterized the magma storage over the entire period of Campi Flegrei activity investigated here. These magmatic environments are ascribable to either mafic or differentiated magmas, stationing in deep and shallow reservoirs, respectively, which interacted frequently, mostly during the last 12 ka of activity. In fact, open-system magmatic processes (mixing/mingling, crustal contamination, $CO_2$ flushing) hypothesized to have occurred before several Campi Flegrei eruptions could have removed earlier-grown crystals from their equilibrium melts. Moreover, our new results indicate that, in the case of complex systems such as Campi Flegrei's, in which different pre-eruptive processes can modify the equilibrium composition of the crystals, one single geothermobarometric method offers little chance to constrain the magma storage conditions. Conversely, combined methods yield more robust results in agreement with estimates obtained in previous independent studies based on both petrological and geophysical methods.

**Keywords:** geothermobarometry; mineral-melt equilibrium; magma storage conditions; Campi Flegrei caldera



**Citation:** Pelullo, C.; Iovine, R.S.; Arienzo, I.; Di Renzo, V.; Pappalardo, L.; Petrosino, P.; D'Antonio, M. Mineral-Melt Equilibria and Geothermobarometry of Campi Flegrei Magmas: Inferences for Magma Storage Conditions. *Minerals* **2022**, *12*, 308. https://doi.org/10.3390/min12030308

Academic Editor: José Francisco Molina

Received: 21 January 2022
Accepted: 25 February 2022
Published: 28 February 2022



## 1. Introduction

The chemical composition of magmatic minerals, combined with the determination of intensive variables (temperature, pressure) recorded by crystals at equilibrium, allows

investigation of the chemicophysical conditions of magmatic systems during storage and prior to eruption (e.g., [1]). The compositional variations in magmatic minerals can be useful to track chemical and physical changes in the magma from which they grew [2–11]. Using experimentally determined phase relationships, e.g., compositions of minerals in equilibrium with a melt as a function of pressure, temperature, water content and oxygen fugacity, the chemical composition of mineral assemblages allows reconstruction of the crystallization conditions. Determination of pre-eruptive conditions in magma plumbing systems through equilibrium relationships between melts and coexisting minerals is one of the major targets of modern petrology. In this context, geothermobarometry allows estimation of crystallization pressure and temperature by applying calibrated equations to the compositions of minerals, matrix glass, melt inclusions and whole rocks, or a combination thereof. The fundamental premise of geothermobarometry is that the mineral assemblage and compositions of a rock are sensitive to pressure and temperature of formation and that the events subsequent to mineral equilibration have not significantly modified these properties [12]. The theoretical basis for most geothermobarometers consists of determining the equilibrium constant for a reaction and estimating the conditions of equilibration based on that value [12,13]. Many geothermometers and geobarometers have been calibrated through experimental data and thermodynamic models. These models are mostly based on exchange reactions between minerals and melt [13–16], cation content in minerals and coexisting melt [17,18], pressure-dependent variations in crystal lattice structure [19–21] or phase relations of a set of minerals [22,23]. Since these models are calibrated for certain mineral phases and restricted magma compositional ranges, the application of a suitable geothermobarometric method depends on the chemical composition of the analyzed rocks and their minerals. For mafic magmas, for example, 'OPAM' (olivine–plagioclase–augite melt) geobarometry uses the composition of a melt in equilibrium with plagioclase, clinopyroxene and olivine to estimate a pressure of 'last equilibration' [22,24]. Some models make use of clinopyroxene components, such as geobarometers based on equations describing the pressure-dependent jadeite-liquid (Jd-liq) reaction, as well as geothermometers based on equations considering the temperature-dependent Jd into diopside–hedenbergite ($Ca(Mg,Fe)Si_2O_6$; Di-Hd) and calcium Tschermak's components ($CaAlAlSiO_6$; Ca-Ts) into Di-Hd exchange reactions [13–15]. Temperature can be determined from coexisting alkali feldspar and plagioclase [13,23,25] and from clino- and orthopyroxene solid solutions [26]. Most of the commonly used geothermometers are based on the modeling of entropy and volume changes occurring in equilibrium reactions between melts and crystals [27]. Clinopyroxene-melt (e.g., [15]) and plagioclase-melt (e.g., [28]) geothermobarometers are well-known and commonly used by petrologists. Based on the composition of the volcanic rocks of interest, when applicable, multiple geothermobarometric models can be employed to provide independent tests. Clinopyroxene-melt geothermobarometry has been used for specific active Italian volcanoes, for example, to define magma storage conditions under Mt. Etna [29]. Likewise, Masotta et al. [30], with the aim of improving the suitability of clinopyroxene-liquid geothermobarometers for evolved alkaline systems, developed and applied recalibrated geothermobarometric equations to Mt. Vesuvius and Campi Flegrei products.

In this work, the geothermobarometers of Putirka [13] and Masotta et al. [30] have been used to estimate pressures and temperatures of crystallization of olivine, clinopyroxene and feldspar crystals from volcanic products belonging to different periods of Campi Flegrei activity. In the last decades, various studies that used different geological, geochemical and/or geophysical information have tried to estimate the depths of magma storage below Campi Flegrei (e.g., [31–50]). Moreover, geothermometric estimates have been performed in several studies (e.g., [51–58]) in order to reconstruct the pre-eruptive temperature conditions of the magmas feeding different eruptions (e.g., Campanian Ignimbrite, Agnano–Monte Spina, Astroni). The temperature values obtained in these studies show largely variable ranges even for rocks of similar composition; moreover, apart from a few studies [30,58], geobarometric estimates are scarce.

The Campi Flegrei volcanic field represents an interesting case study where different geothermobarometers can be applied in order to: (i) estimate the storage depths at which the magmas stationed before single eruptive events or a cycle of events; (ii) reconstruct periods of shift in magma storage conditions; and (iii) unravel the evolution through time of its magmatic feeding system. All these outcomes would have a deep impact on the understanding of the behavior of the magmatic plumbing system that feeds Campi Flegrei, one of the highest-risk active volcanic areas on Earth for its high population density.

## 2. The Campi Flegrei Volcanic Field

The Campi Flegrei volcanic field, together with the Somma–Vesuvius stratovolcano and Ischia volcanic island, is one of the three active volcanoes of the Neapolitan area. Its morphology is dominated by a 12 km-wide caldera depression (Figure 1), resulting from multiple collapses related to two highly explosive volcanic eruptions: the Campanian Ignimbrite (CI) occurring *c.* 40 ka [59,60] and the Neapolitan Yellow Tuff (NYT) occurring *c.* 15 ka [61].

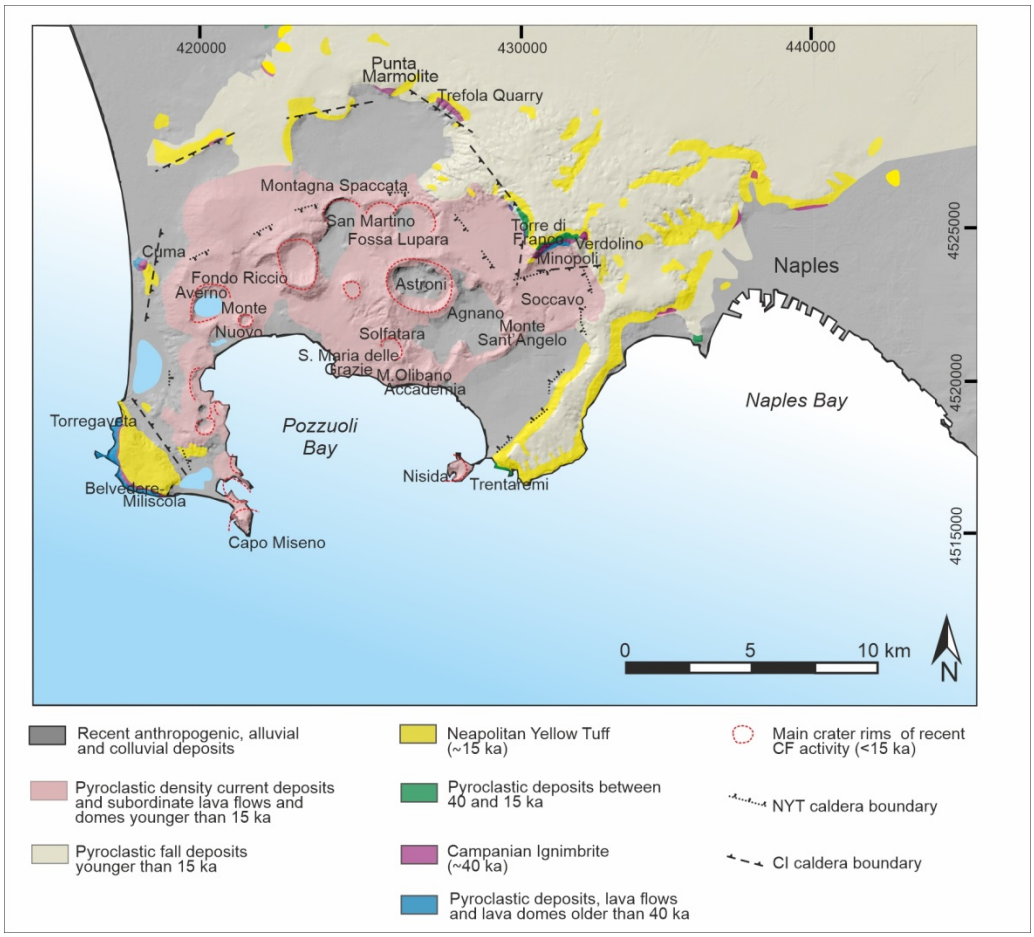


**Figure 1.** Simplified geological map of the Campi Flegrei caldera showing the traces of regional faults and main morphological structures such as caldera, crater rims and faults (modified after [62]).

The volcanic activity has been dominantly explosive through time and has mostly led to the emplacement of pyroclastic rocks with subordinate lava flows and domes. The age of the beginning of volcanism in the area is not well-constrained. Old ignimbrites, even if highly altered, at Durazzano (116.1 ka), Moschiano (184.7 ka), Seiano Valley (245.9 and 289.6 ka) and Taurano–Acqua Feconia (157.4, 183.8, 205.6 and 210.4 ka) localities, in different sites of the Campania Plain, have been characterized by De Vivo et al. [63], Rolandi et al. [64] and Belkin et al. [65]. At least twelve pre-CI units are recognized at the Trefola Quarry [66] spanning the 59–39 ka period [67]. The CI, emplaced during a

catastrophic explosive event having a magnitude of 7.2 [68], is considered the most powerful eruption ever to occur in the Neapolitan area. The CI Plinian eruption emplaced a large volume (~80 to 300 $km^3$ dense rock equivalent; [68–71]) of pyroclastic fall and pyroclastic-density-current products, which resulted in a very complex sequence in proximal, medial and distal outcrops [69,72–78], as well as a co-ignimbrite ash fall dispersed in the eastern Mediterranean Sea and eastern Europe (e.g., [75,79,80]). Post-CI/pre-NYT volcanic activity was confined inside the CI caldera and the majority of the eruptions were produced by explosive, mostly hydromagmatic activity [66]. $^{40}Ar/^{39}Ar$-dated eruptions range in age from 30.3 ka to 14.6 ka [67]. Moreover, Albert et al. [81] recently revealed the high magnitude (M 6.6 or VEI 6) of one of the pre-NYT deposits: the Masseria del Monte Tuff, dated at 29.3 ± 0.7 ka. The NYT (14.9 ka; [61]) was produced during the last largest eruption of the Campi Flegrei caldera, and it is by far the largest trachytic phreatoplinian deposit known to date. The NYT outcrops in scattered localities over an area of ~1000 $km^2$, with a conservatively estimated volume of ~40 $km^3$ (DRE; [82–84]).

During the last 15 ka, intense volcanism and deformation affected the caldera. This period has been divided into three epochs of activity: epoch 1—*c.* 15–10.6 ka; epoch 2—*c.* 9.6–9.1 ka; and epoch 3—*c.* 5.5–3.5 ka [85]. During epoch 1, at least 32 magmatic-to-phreatomagmatic explosive eruptions took place, with a mean frequency of one eruption every 70 years [86]. Among these, the Minopoli 1, Soccavo 4, Minopoli 2, Fondo Riccio and Montagna Spaccata eruptions have been subject of recent studies (e.g., [87–89]). Close to the end of this phase, the Plinian deposit of the Pomici Principali eruption was emitted from the Agnano area (11.9–12.1 ka; [85]). During epoch 2, six low-magnitude explosive eruptions took place with a mean frequency of 65 years [86,90]. During epoch 3, an intense monogenetic explosive and subordinate effusive activity took place; the principal events that modified the morphological setting of the volcanic field were the emplacements of Solfatara (4.1–4.3 ka; [85]), Astroni (4.1–3.8 ka; [85–91]), Averno (5.4–4.1 ka; [85,92,93]), Nisida (4.1–3.2 ka; [85,94]) and Monte Nuovo (1538 AD; [48,95–97]) pyroclastic cones, the Agnano Monte Spina (4.4–4.6 ka; [85,98–102]) Plinian magmatic-to-phreatomagmatic eruption and Monte Olibano and Accademia lava domes (4.36 ± 1.13 ka; [103]). The last event took place in 1538 AD, with the formation of Monte Nuovo scoria cone ([48] and reference therein).

The intense fumarolic activity and the ground deformation episodes that occurred in recent decades (e.g., [104]) testify to the persistent activity of the Campi Flegrei magmatic system that remains in a state of unrest (e.g., [105–107]). The presence of 350,000 inhabitants in the central part of the caldera raises the risk level to very high [108,109].

The Campi Flegrei volcanic field erupted alkaline potassic rocks ranging in composition from trachybasalt to phonotrachyte, with a predominance of trachyte (Figure 2; [67,110,111]).

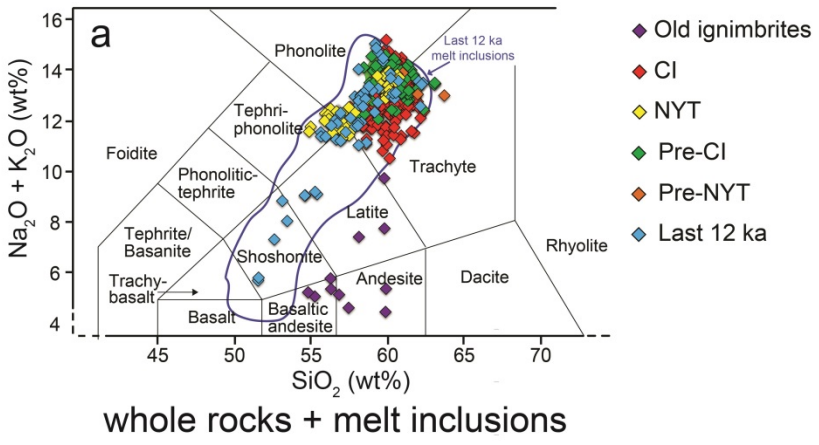


**Figure 2.** *Cont.*

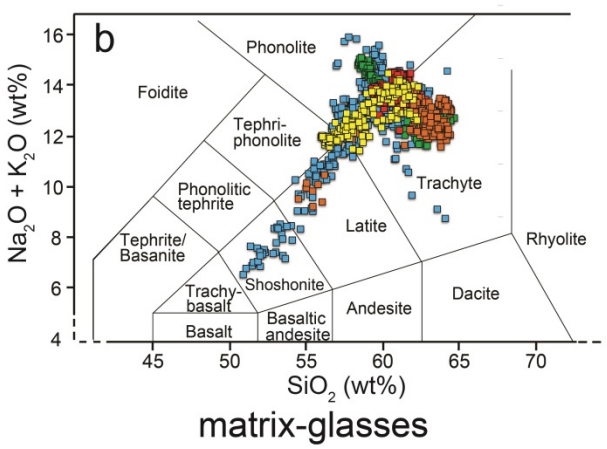


**Figure 2.** TAS (Total alkali vs. silica) diagram for the classification of the Campi Flegrei (**a**) whole rocks, melt inclusions and (**b**) matrix-glasses. Whole-rock, melt-inclusion and matrix-glass analysis of rocks that were erupted in different periods of Campi Flegrei's volcanic activity are plotted. Data from Melluso et al. [51], Orsi et al. [83], Civetta et al. [52], de Vita et al. [98], Signorelli et al. [112], Pappalardo et al. [72,113], Webster et al. [114], Fulignati et al. [53], Munno and Petrosino [115], D'Oriano et al. [116], Marianelli et al. [117], Piochi et al. [95], Cannatelli et al. [87], Fowler et al. [118], Fedele et al. [69,119], Mangiacapra et al. [88], Arienzo et al. [94,101,120], Formentraux et al. [121], Tomlinson et al. [122], Belkin et al. [65], Forni et al. [55,56,89] and Iovine et al. [57]. Whole-rock analyses of the old ignimbrites are affected by alteration.

Most of the products older than 15 ka, except for a few rocks that were erupted during the pre-NYT period (Torregaveta and Masseria del Monte Tuff), exhibit the most evolved compositions (trachytes and phonotrachytes; Figure 2). At the end of the first epoch of the last 15 ka of activity, less-differentiated magmas (trachybasalt and latite) were erupted along NE–SW regional tectonic structures (e.g., [66,110]).

## 3. Materials and Methods

New compositional data on olivine, clinopyroxene, plagioclase and K-feldspar phenocrysts from products representative of some pre-CI eruptive units and of the last 5 ka's Agnano–Monte Spina and Astroni eruptions have been collected (Supplementary Materials Table S1). Major- and minor-element (Si, Ti, Al, Fe, Mn, Mg, Ca, Na and K) contents of phenocrysts were acquired at the HP-HT Laboratory of Experimental Volcanology and Geophysics of the Istituto Nazionale di Geofisica e Vulcanologia in Rome (Italy), using a Jeol-JXA8200 electron microprobe equipped with five wavelength-dispersive spectrometers. Crystals in carbon-coated resin mounts were analyzed under high-vacuum conditions, using an accelerating voltage of 15 kV, with a beam diameter of 5 µm. The electron-beam current was set at 7.5 nA. Elemental counting times were 10 s on the peak and 5 s on each of two background positions. Corrections for interelemental effects were made using a ZAF (Z: atomic number; A: absorption; F: fluorescence) routine. The range of standards for calibration was taken from Micro-Analysis Consultants (MAC) and variable diffraction devices: albite (Si-PET, Al-TAP, Na-TAP), forsterite (Mg-TAP), augite (Fe-LIF), apatite (Ca-PET), orthoclase (K-PET), rutile (Ti-PET) and rhodonite (Mn-LIF). Accuracy was better than 1–5% except for elements with abundances below 1 wt%, for which it was better than 5–10%. Precision was typically better than 1–5% for all analyzed elements.

For the aim of this work, the newly acquired data were integrated with a suitably created database of the chemical composition of mineral phases from different periods of Campi Flegrei's volcanic activity. We retrieved major and minor element contents of olivine, clinopyroxene, plagioclase and alkali-feldspar phenocrysts and microphenocrysts from previous works [51–53,55–57,65,69,72,83,87–89,94,95,98,101,113–122] in which these mineral phases were analyzed. When available, the whole-rock, matrix-glass and melt-

inclusion compositions have been also included in the database. These were used as representative of melt compositions for the evaluation of equilibria and for the application of geothermobarometers.

The collected data belong to different periods of activity of the Campi Flegrei volcanism, that have been divided into: old ignimbrites—*c.* 290–115 ka [65]; pre-CI—*c.* 59–47 ka [67,103]; CI—*c.* 40 ka [59,60]; pre–NYT—*c.* 30–16 ka [67,103]; NYT—*c.* 15 ka [61]. As for the recent period of activity (last 15 ka), since there are no data on volcanic products erupted during the 15–13 ka time interval, we consider the last 12 ka, starting with the Pomici Principali eruption (12.1–11.9 ka; [85]).

## 4. Results

### *4.1. Mineral Chemistry*

#### 4.1.1. Olivine

Olivine crystals mostly occur in the products belonging to the last 12 ka of volcanic activity. In particular, this mineral phase is found in volcanic rocks emplaced during the Minopoli 1, Pomici Principali, Minopoli 2, Fondo Riccio and Astroni eruptions. Their MgO and FeO contents range from 50 to 43 wt% and from 19 to 10 wt%, respectively. Their CaO contents range between 0.5 and 0.2 wt%. The olivine phenocrysts range in composition from $Fo_{90}$ to $Fo_{80}$ (Forsterite mol %; Figure 3), showing a limited compositional variation.

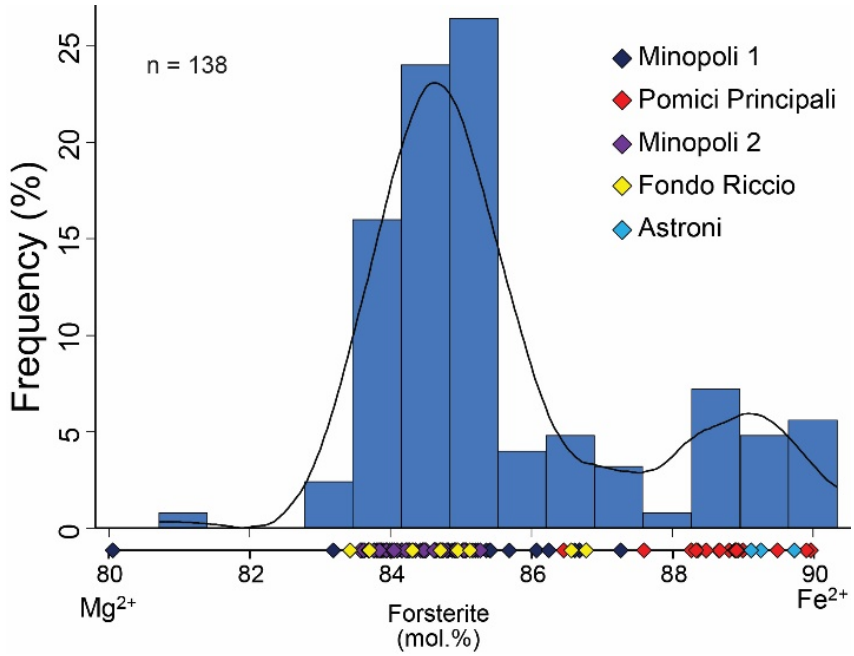


**Figure 3.** Forsterite (mol %) contents of the Campi Flegrei olivine and Fo (mol %) frequency histogram showing the distribution of olivine compositions.

The Forsterite (mol %) contents of olivine show a bimodal distribution (Figure 3), characterized by (1) the most frequent compositional population ranging between $Fo_{87}$ and $Fo_{84}$ and (2) a less frequent compositional population ranging between $Fo_{90}$ and $Fo_{88}$. On the other hand, olivine microlites occurring in the groundmass of several lava domes (Cuma; 45.9 ±3.6 ka; Wu et al. [103]; Punta Marmolite; 47 ka; Accademia; 3.9 ka; Melluso et al. [111] and references therein) show a wider compositional range ($Fo_{90–1}$) with respect to those of the phenocrysts belonging to explosive volcanic activity, studied in this work. The olivines belonging to such relatively scarce Campi Flegrei effusive products also show fayalite- and tephroite-rich compositions [111].

4.1.2. Clinopyroxene

Clinopyroxene occurs in all volcanic products belonging to the Campi Flegrei eruptions, and mostly classifies as diopside and Fe-rich diopside ($Wo_{52–41}En_{51–29}Fs_{25–4}$; Wollastonite–Enstatite–Ferrosilite; Figure 4a–c). Those belonging to rocks erupted after the NYT eruption show compositions also richer in Fe ($Wo_{53–44}En_{50–14}Fs_{32–4}$), e.g., hedenbergite.

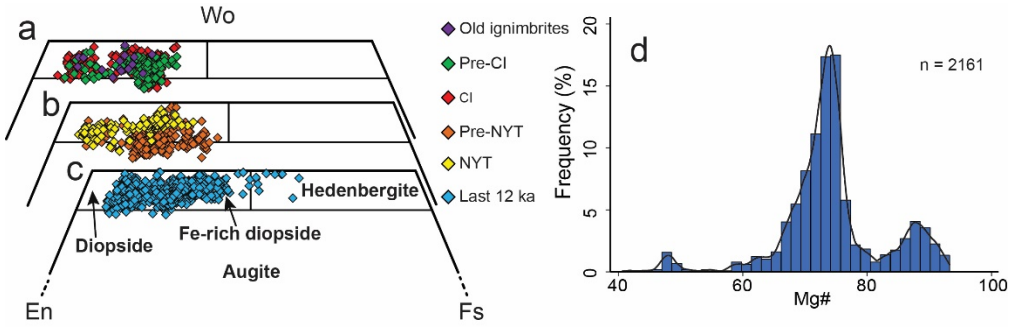


**Figure 4.** Di-Hd-En-Fs (**a**–**c**) classification diagram and (**d**) Mg# frequency histogram showing the distribution of Campi Flegrei clinopyroxene composition. Di = diopside; Hd = hedenbergite; En = enstatite; Fs = ferrosilite.

The Mg# [molar $Mg^{2+}/(Mg^{2+} + Fe_{tot}) \times 100$] ranges from 92 to 40 (Figure 4d). This parameter reflects a compositional polymodality in the clinopyroxene phenocrysts of volcanic rocks belonging to all periods of activity. Clinopyroxenes of rocks belonging to the different periods of activity show variable range of Mg# (Table 1), in particular those from rocks emplaced during the last 12 ka cover the whole range of values (Mg# = 92–41; Figure 5).

**Table 1.** Ranges of Mg# values of clinopyroxene crystals belonging to different periods of Campi Flegrei activity.

| Eruptive Period | Clinopyroxene Mg# |
|---|---|
| Old ignimbrites | 89–67 |
| Pre–CI | 91–61 |
| CI | 92–62 |
| Pre–NYT | 91–55 |
| NYT | 92–61 |
| Last 12 ka | 92–41 |

The correlations between Mg# and Al, Ti, Na, Mn and Cr contents show some changes/kinks along the whole continuous compositional variation. Moreover, the clinopyroxenes of rocks erupted during the last 12 ka show chemical variation trends different to those of clinopyroxenes of rocks erupted during previous periods (Figure 5). These features are described in detail below.

$TiO_2$ and $Al_2O_3$ contents of clinopyroxenes range from 2.90 to 0.10 wt% and from 9.62 to 0.73 wt%, respectively (Figure 5a,b). $Na_2O$ and MnO contents range from 1.36 to 0.03 wt% and from 3.23 to 0.01 wt% (Figure 5c,d). $Cr_2O_3$ content ranges from 1.00 to 0.01 wt% (Figure 5e). $Na_2O$, $TiO_2$ and MnO contents increase with the decrease in Mg#. In particular, the $Na_2O$ and MnO contents increase linearly with the decrease in Mg# from 92 to 80 and then increase exponentially with the decrease in Mg# from 80 to 55 (Figure 5c,d). An exception are some clinopyroxenes belonging to rocks of the last 12 ka, in which the $Na_2O$ and MnO contents are on average lower and continue to increase linearly with respect to the whole Mg# range. $Cr_2O_3$ and $SiO_2$ contents decrease as Mg# decreases (Figure 5e,f). The $Cr_2O_3$ contents decrease exponentially with the decrease in Mg# from 92 to 80 and

then decrease linearly as Mg# decreases from 80 to 41. The $Al_2O_3$ contents increase with the decrease in Mg# from 92 to 80, then decrease with the decrease in Mg#, except for the crystals of volcanic products belonging to the last 12 ka, in which the $Al_2O_3$ contents continue to increase as Mg# decreases (Figure 5a).

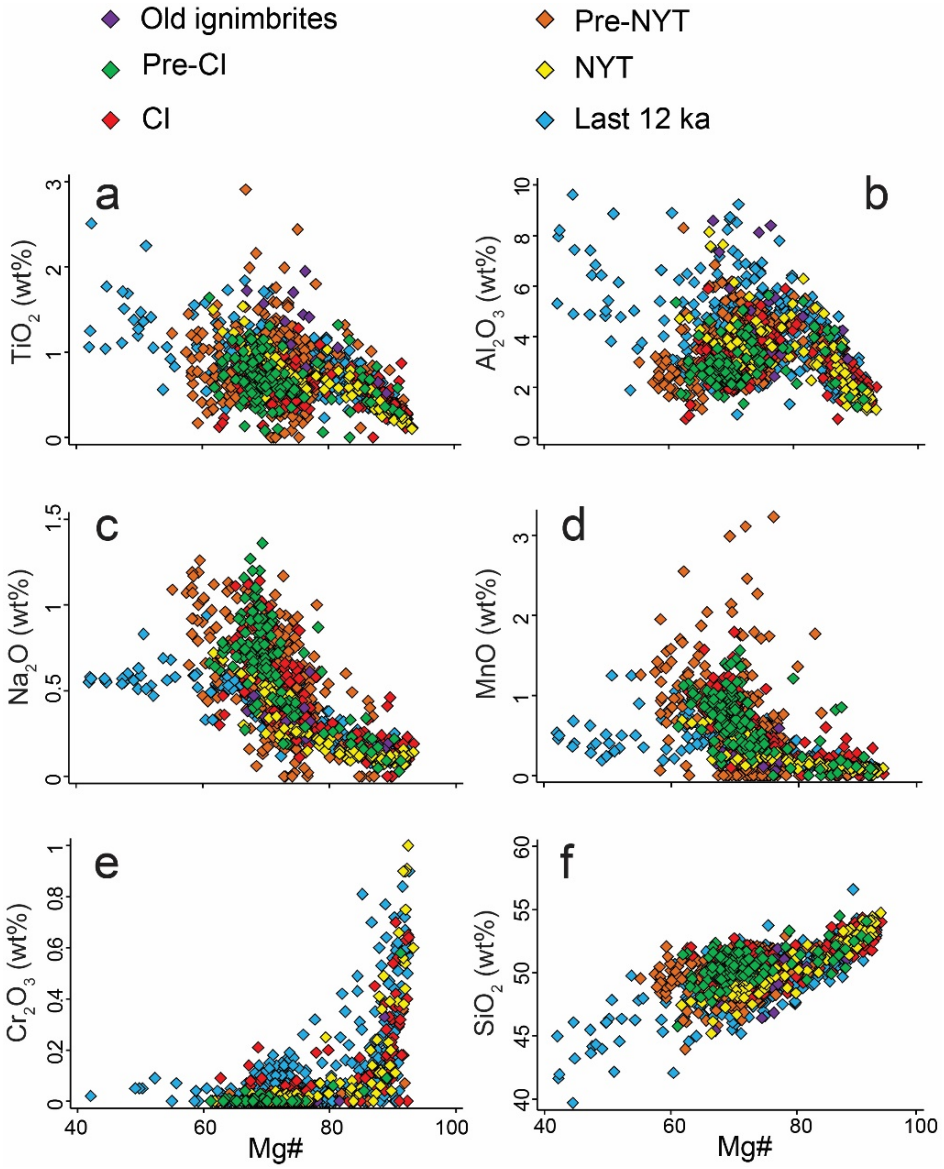


**Figure 5.** (**a**) Mg# vs. $TiO_2$, (**b**) Mg# vs. $Al_2O_3$, (**c**) Mg# vs. $Na_2O$, (**d**) Mg# vs. MnO, (**e**) Mg# vs. $Cr_2O_3$, and (**f**) Mg# vs. $SiO_2$ of clinopyroxene crystals from volcanic products belonging to different periods of Campi Flegrei's activity.

Similarly to olivine, the clinopyroxenes occurring in the groundmass of the Campi Flegrei lavas show wide compositional variations (Mg# = 89–1), covering the complete spectrum from Mg- to Fe-rich compositions and reaching Na- and Zr-rich compositions (e.g., aegirine; [111]).

#### 4.1.3. Feldspars

Feldspar is a ubiquitous phase in the volcanic products of Campi Flegrei. K-feldspar is the most abundant phase in the pyroclastic rocks, belonging to all periods of activity, mostly in trachytes. Plagioclase mostly occurs in volcanic rocks representative of poorly evolved magmas. The plagioclase and alkali-feldspar crystals belonging to the different periods of

activity cover wide compositional ranges, except for plagioclases from the pre-NYT and NYT periods (Figure 6a–c; Table 2).

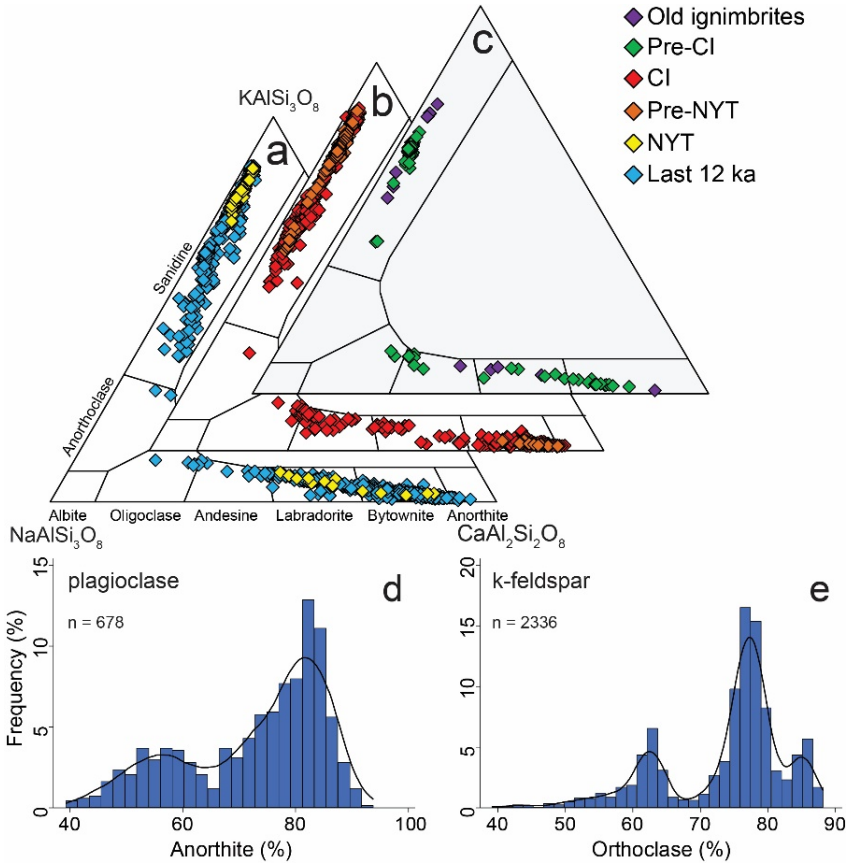


**Figure 6.** (**a**–**c**) An-Ab-Or classification diagram of feldspars; (**d**) An (mol %) and (**e**) Or (mol %) frequency histograms showing the distribution of Campi Flegrei feldspar composition.

**Table 2.** Plagioclase and K-feldspar composition of products emplaced during different Campi Flegrei periods of activity. An = anorthite; Ab = albite; Or = orthoclase.

| Eruptive Period | Plagioclase Composition | K-Feldspar Composition |
|---|---|---|
| Old ignimbrites | $An_{88–49}Ab_{44–10}Or_{6–1}$ | $Or_{74–50}$ |
| Pre-CI | $An_{82–24}Ab_{64–16}Or_{11–2}$ | $Or_{67–54}$ |
| CI | $An_{90–25}Ab_{62–8}Or_{14–1}$ | $Or_{88–42}$ |
| Pre-NYT | $An_{89–76}Ab_{20–9}Or_{3–1}$; | $Or_{87–51}$ |
| NYT | $An_{86–47}Ab_{43–12}Or_{8–2}$ | $Or_{86–72}$ |
| Last 12 ka | $An_{94–40}Ab_{51–5}Or_{18–1}$ | $Or_{87–39}$ |

The Campi Flegrei plagioclase shows a bimodal distribution, reflected in the An (mol %) content, characterized by a main compositional population exhibiting $An_{90–63}$ and a second population exhibiting $An_{62–40}$ (Figure 6d). Likewise, the frequency histogram of sanidine composition (Or mol. %; Figure 6e) shows two main compositional populations: the most frequent is in the range $Or_{88–68}$, whereas a second population is characterized by composition in the range $Or_{67–40}$.

### *4.2. Mineral-Melt Equilibrium*

The equilibria between melt and selected minerals were investigated using (i) the Fe-Mg exchange coefficient for olivine and clinopyroxene, hereafter referred to as equi-

librium test 1; (ii) the comparison between observed and predicted normative diopside–hedenbergite (DiHd) components for clinopyroxene, hereafter referred to as equilibrium test 2; (iii) the Or-Ab partitioning coefficient for alkali feldspar, hereafter referred to as equilibrium test 3; and (iv) the An-Ab partitioning coefficient for plagioclase, hereafter referred to as equilibrium test 4. For the evaluation of the equilibrium, Campi Flegrei melt-inclusion, whole-rock and matrix-glass analyses were used as representative of the composition of various melts.

#### 4.2.1. The "Classic" Method for Assessing Equilibrium between Olivine or Clinopyroxene and Their Melt: The $^{Fe\text{-}Mg}Kd_{min\text{-}liq}$ Exchange Coefficient (Test 1)

Equilibrium test 1 is the most commonly used test for assessing equilibrium between clinopyroxene or olivine and melt pairs. It consists of the evaluation of the Fe-Mg partitioning between mineral and liquid, known as the Fe-Mg exchange coefficient, defined as $^{Fe\text{-}Mg}Kd_{min\text{-}liq} = (MgO_{liq}FeO_{min})/(MgO_{min}FeO_{liq})$, where "liq" is the liquid; "min" is the mineral; and MgO and FeO are molar fractions (e.g., Roeder and Emslie, 1970; Putirka, 2005, 2008). In this case, the equilibrium conditions are verified when the Fe-Mg partitioning between olivine and host rock ($^{Fe/Mg}Kd_{Ol\text{-}liq}$) is 0.30 ± 0.03 [123,124], and when the Fe-Mg partitioning between clinopyroxene and host rock ($^{Fe/Mg}Kd_{Cpx\text{-}liq}$) is 0.27 ± 0.03 (e.g., [15,125]). In a Rhodes diagram ($Mg\#_{mineral}$ vs. $Mg\#_{melt}$), the lines joining points satisfying these conditions define the theoretical equilibrium field (Figure 7).

Concerning the Campi Flegrei olivines, only a few olivines from Fondo Riccio and Minopoli 2 are in the equilibrium field (Figure 7a). As for the clinopyroxenes, a few crystals from rocks belonging to different periods of activity are in equilibrium with their melts (Figure 7b–i).

#### 4.2.2. An Alternative Equilibrium Test for Clinopyroxene: The Measured versus Predicted Components (Test 2)

An alternative and more robust test for assessing the equilibrium between a mineral and coexisting melt is what we call equilibrium test 2, which consists of the comparison between normative mineral components predicted for a mineral phase from melt composition, and those measured in the analyzed crystals (e.g., [13–126]). Since all the studied clinopyroxenes are diopsidic in composition, we take into account the Di and Hd components. These were calculated following the scheme proposed by Putirka et al. [14] and Putirka [13]. The predicted clinopyroxene components based on melt composition were calculated using equation 3.1a in Putirka [127]: $\ln[DiHd^{cpx}] = -9.8 + 0.24\ln[Ca^{liq}(MgO + FeO^{liq})(Si^{liq})^2] + 17{,}558/T + 8.7\ln(1670/T) - 4.61 \times 10^3[(EnFs^{cpx})^2/T]$.

Only one crystal from the old ignimbrites (Taurano ignimbrite) results in equilibrium (Figure 8a); nevertheless, we discarded these products since they were altered and, therefore, the rock composition was almost surely affected by intense weathering processes [65]. A few clinopyroxenes from all deposits belonging to the pre-CI period are in equilibrium with their melts (Figure 8b). Some crystals from the CI also are in the equilibrium field (Figure 8c). For the pre-NYT period, some clinopyroxenes result in equilibrium conditions (Figure 8d). Several crystals from the NYT are also in the equilibrium field (Figure 8e). For the last 12 ka, some crystals from Minopoli 1, Minopoli 2, Soccavo 4, Averno and Monte Nuovo eruptions and a few crystals from Pomici Principali, Fondo Riccio, Capo Miseno, Agnano–Monte Spina, Astroni and Nisida eruptions are in equilibrium with their melts (Figure 8f–h).

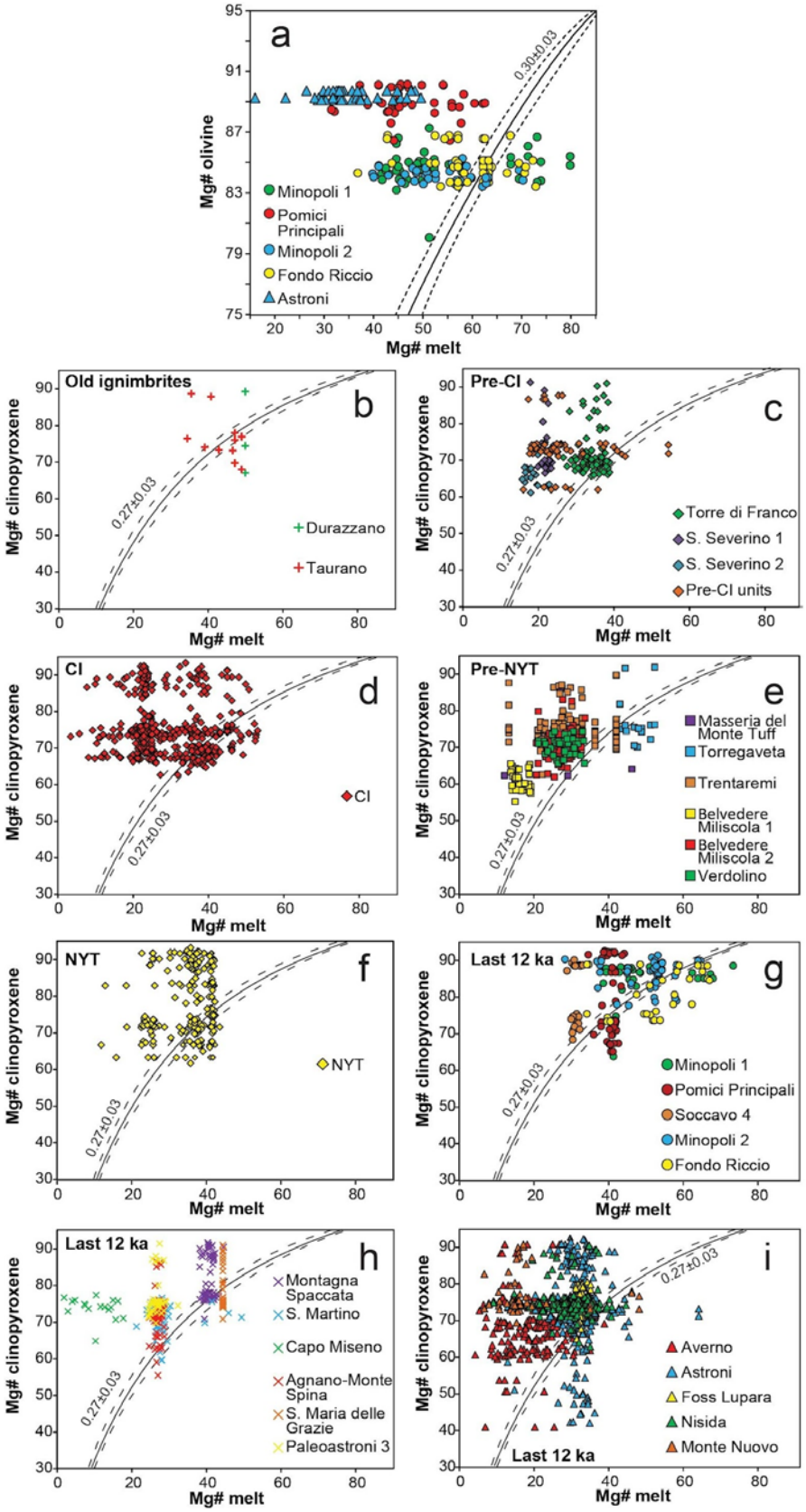


**Figure 7.** Equilibrium test 1 based on the Fe-Mg partitioning between olivine or clinopyroxene and melt ($^{Fe\text{-}Mg}Kd_{ol\text{-}liq}$ = 0.30 ± 0.03 and $^{Fe\text{-}Mg}Kd_{cpx\text{-}liq}$ = 0.27 ± 0.03 [13,15,28,123,125] for Campi Flegrei products of variable age. (**a**) olivine-melt equilibrium test; clinopyroxene-melt equilibrium tests for products belonging to Old ignimbrites (**b**), Pre-CI (**c**), CI (**d**), Pre-NYT (**e**), NYT (**f**) and last 12 ka (**g**–**i**).

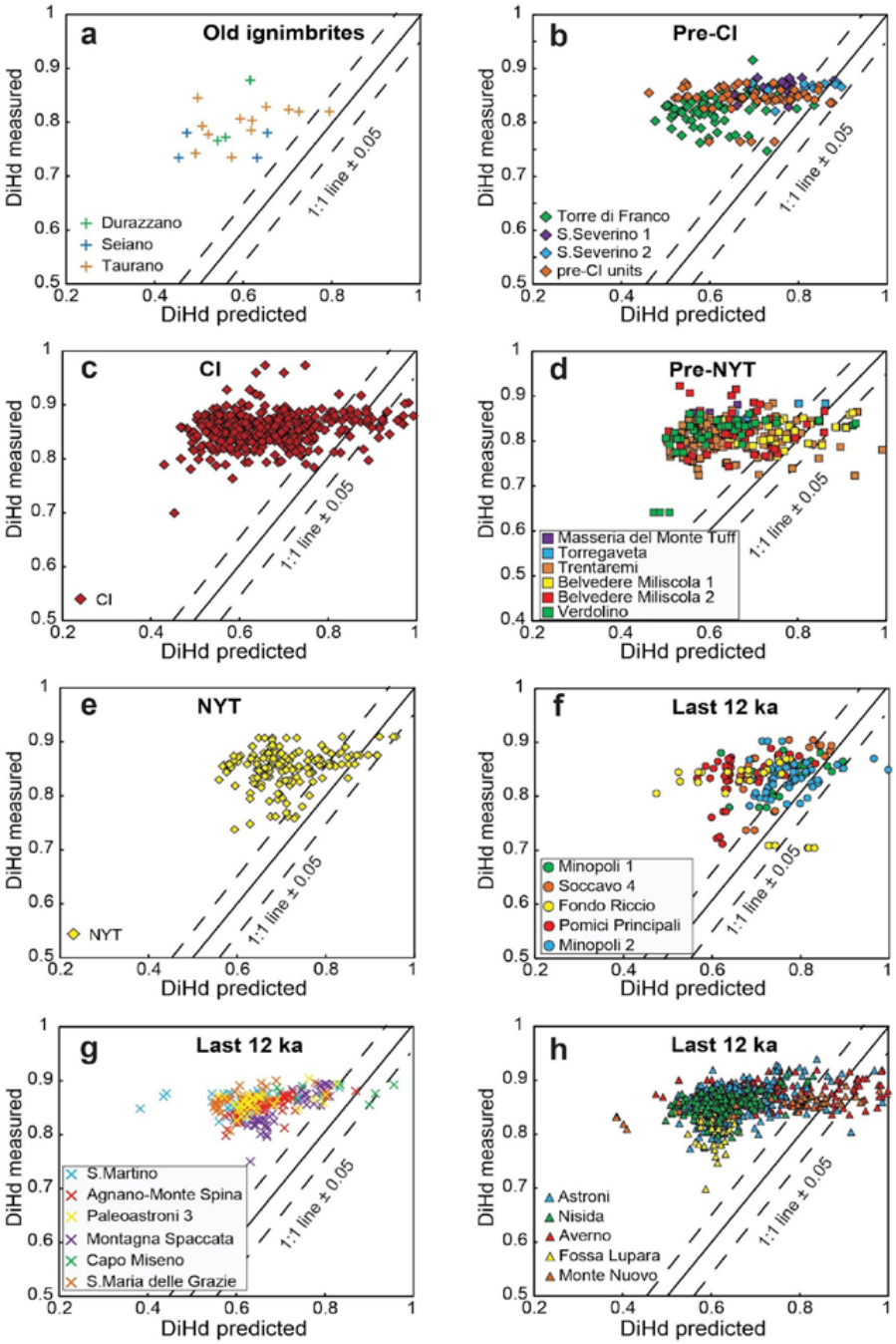


**Figure 8.** Equilibrium test 2 based on the comparison between measured and predicted clinopyroxene components, i.e., Di + Hd between crystal and melt from equilibrium values [126] for Campi Flegrei products belonging to Old ignimbrites (**a**), Pre-CI (**b**), CI (**c**), Pre-NYT (**d**), NYT (**e**) and last 12 ka (**f**–**h**).

#### 4.2.3. Equilibrium Tests for Alkali-Feldspar and Plagioclase (Tests 3 and 4)

For K-feldspar, equilibrium test 3 used here is based on Or–Ab partitioning between K-feldspar and melt (e.g., [13,128]), known as the Or-Ab exchange coefficient, defined as $^{\text{K-feld-melt}}Kd_{\text{Or-Ab}} = Na_{\text{Feld}} \times XAl_{\text{liq}} \times XCa_{\text{liq}}/XCa_{\text{Feld}} \times XNa_{\text{liq}} \times XSi_{\text{liq}}$ vs. predicted $^{\text{K-feld-melt}}Kd_{\text{Or-Ab}} = -0.67 + (K_{\text{liq}}/K_{\text{Feld}}{}^2 + \ln(\exp(K_{\text{liq}}{}^2/Na_{\text{liq}} + K_{\text{liq}})/10$, according to the approach by Mollo et al. [128]. In a measured vs. predicted $Kd_{\text{Or-Ab}}$ diagram, the equilibrium field is shown inside the 1:1 line ± 0.25 (Figure 9).

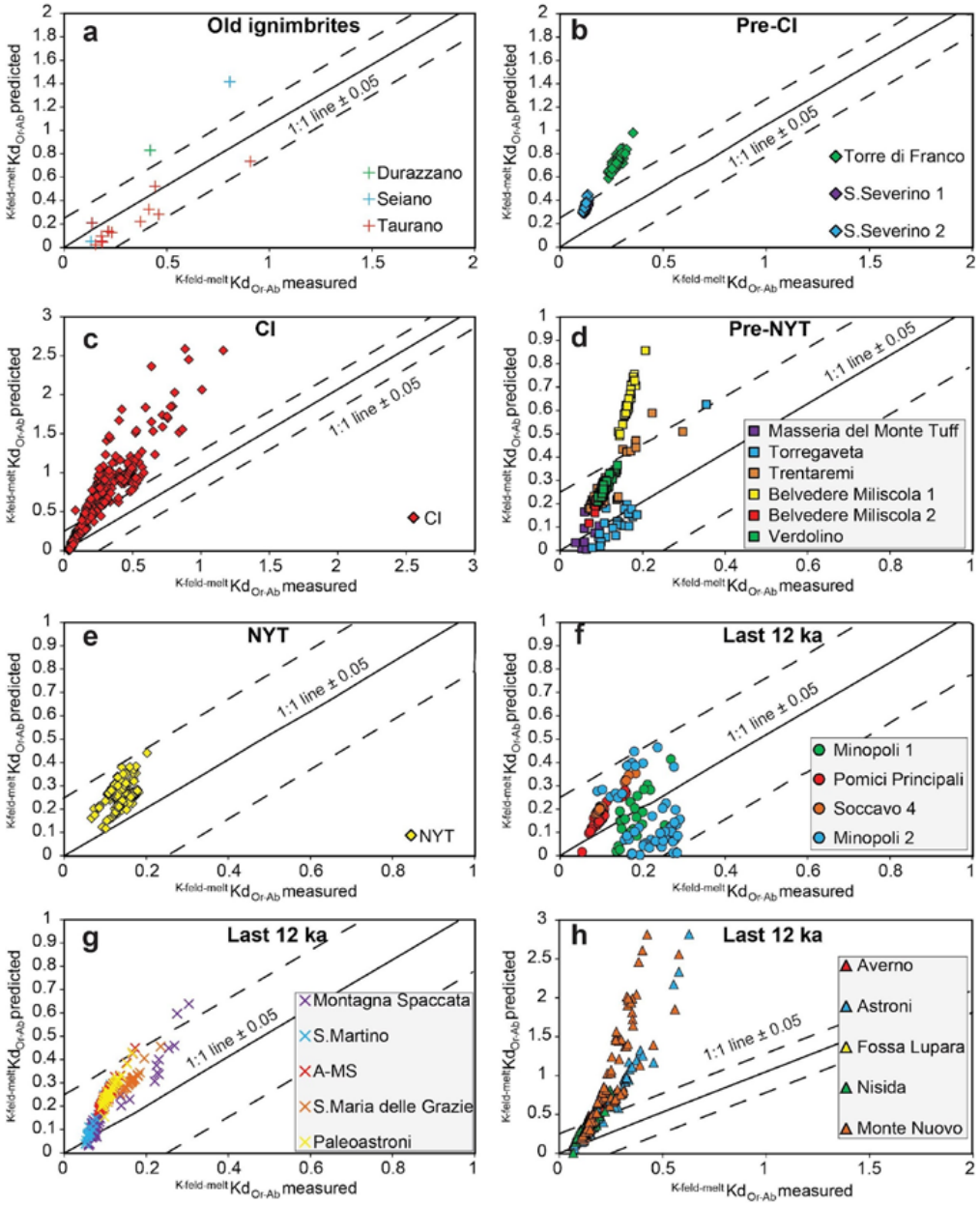


**Figure 9.** $^{kfeld-liq}Kd_{Or\text{-}Ab}$ equilibrium test 3 based on Or-Ab exchange between K-feldspar and liquid [128] for Campi Flegrei feldspars belonging to Old ignimbrites (**a**), Pre-CI (**b**), CI (**c**), Pre-NYT (**d**), NYT (**e**) and last 12 ka (**f**–**h**); the equilibrium field is inside the 1:1 line ± 0.25.

We do not consider the equilibrium relationships between K-feldspars and host rocks from the old ignimbrites that are altered (Figure 9a). For the pre-CI period, crystals from the S. Severino 1 and S. Severino 2 eruptions are in the equilibrium field, whereas those from the Torre di Franco eruption are not (Figure 9b). Several crystals from the CI eruption are in equilibrium with their melts (Figure 9c). All K-feldspars erupted in the pre-NYT period, except those from Belvedere Miliscola 1 and some from Trentaremi eruptions, are in the equilibrium field (Figure 9d). All K-feldspars from the NYT eruption are in equilibrium with their melts (Figure 9e). For the products erupted during the last 12 ka, apart from some crystals from the Montagna Spaccata, Astroni and Monte Nuovo eruptions, all the K-feldspars are in equilibrium conditions (Figure 9f–h).

The equilibrium conditions for plagioclase were tested via equilibrium test 4, which is based on the partitioning of An-Ab between mineral and melt. This is known as An-Ab exchange coefficient defined as $^{pl\text{-}melt}Kd_{Ab\text{-}An} = (XNa_{Plag} \times XAl_{liq} \times XCa_{liq})/(XCa_{Plag} \times$

$XNa_{liq} \times XSi_{liq}$) where "liq" is the liquid composition, "Plag" is the plagioclase composition, and all components are expressed as molar fractions (e.g., [13]). The variation diagram of An (mol %) vs. calculated $^{pl\text{-}melt}Kd_{Ab\text{-}An}$ shows the plagioclase-melt stability field drawn using a value for $^{pl\text{-}melt}Kd_{Ab\text{-}An}$ of 0.1 ± 0.05 (Figure 10; [13]).

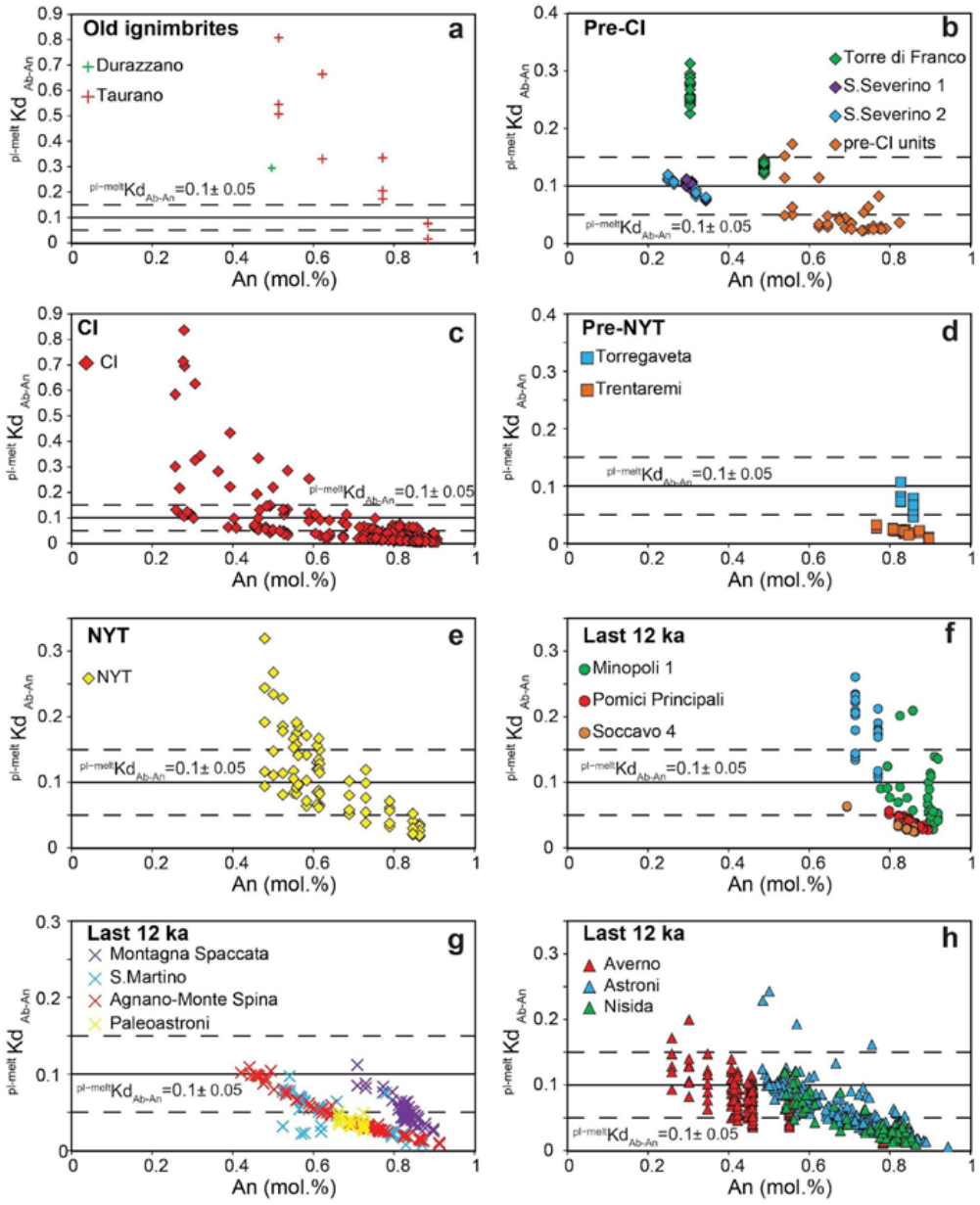


**Figure 10.** Equilibrium test 4: variation diagram of An (mol %) vs. calculated $^{pl\text{-}melt}Kd_{Ab\text{-}An}$, for Campi Flegrei plagioclases belonging to Old ignimbrites (**a**), Pre-CI (**b**), CI (**c**), Pre-NYT (**d**), NYT (**e**) and last 12 ka (**f**–**h**). The plagioclase-melt stability field was drawn using a value for $^{pl\text{-}melt}Kd_{Ab\text{-}An}$ of 0.1 (continuous line) ± 0.05 (dotted lines; e.g., [13]).

Even in this case, we do not take into account the plagioclase-melt equilibria for the old ignimbrites (Figure 10a). For the pre-CI period, all crystals from the S. Severino 1 and S. Severino 2 eruptions and a few crystals from other pre-CI units are in equilibrium with their melts (Figure 10b). Several plagioclases from the CI are also in the equilibrium field (Figure 10c). For pre-NYT units, all crystals belonging to the Torregaveta eruption are in equilibrium, whereas those from Trentaremi eruption are not (Figure 10d). Most of plagioclases in the range $An_{85–50}$ from the NYT eruption are in equilibrium (Figure 10e). For the products of the last 12 ka, some plagioclase crystals from Minopoli 1, Minopoli 2,

Pomici Principali, Montagna Spaccata, S. Martino, Agnano–Monte Spina, Averno, Astroni and Nisida eruptions result in equilibrium with their host melts (Figure 10f–h).

### *4.3. Geothermobarometric Estimates*

We applied various geothermometers and geobarometers to all the mineral-melt couples which passed the equilibrium tests based on the $^{Fe\text{-}Mg}Kd_{min\text{-}liq}$ (olivine and clinopyroxene) and on the comparison between measured and predicted components (clinopyroxene and feldspar). Some geothermobarometers require the $H_2O$ (wt%) content as an input parameter, which can affect the output T–P estimates. Hence, in cases where melt-inclusion compositions have been used as representative of melts in equilibrium with crystals, the volatile contents used are exactly those detected in melt inclusions of the erupted products; in cases where the whole-rock or matrix-glass compositions have been used as representative of melts, the $H_2O$ analyzed in the whole rock or the water content obtained by difference has been used.

As shown before (Section 4.2), a few olivine crystals passed the equilibrium test. On these, we applied Equation (4) [T = (15,294.6 + 1318.8P + 2.4834 $(P)^2$)/(8.048 + 2.8352 ln $D^{ol\text{-}liq}_{Mg}$ + 2.047 ln 1.5 ($X^{Mg}_{liq}$ + $X^{Fe2+}_{liq}$ + $X^{Ca}_{liq}$ + $X^{Mn}_{liq}$) + 2.575 ln ($3X^{Si}_{liq}$) − 1.41 7/2ln(1 − $X^{Al}_{liq}$) + 7ln(1 − $X^{Ti}_{liq}$) + 0.222 $H_2O_{liq}$ + 0.5 P] of the olivine-melt geothermometer of Putirka et al. [129], commonly used for hydrous melts, and whose standard error of estimate (SEE) is 29 °C (e.g., [13]). Two olivine-melt pairs from Minopoli 1 yield temperatures of 1065 and 1060 °C (Figure 11a). The output temperature estimates for the Minopoli 2 olivines range between 1122 and 1045 °C, with an average of 1102 ± 20 °C. The Fondo Riccio olivines in equilibrium with their melts yield temperature estimates in the range of 1175–922 °C, with an average of 1005 ± 84 °C.

For clinopyroxenes resulting in equilibrium with their melts via equilibrium test 1, we used the geothermobarometers of Putirka [13] and Masotta et al. [30]. Specifically, we applied the Equation (33) [$10^4$/T = 7.53 − 014 ln ($X^{cpx}_{Jd}X^{liq}_{CaO}X^{liq}_{FeO+MgO}/X^{cpx}_{DiHd}X^{liq}_{Na}X^{liq}_{Al}$) + 0.07 ($H_2O^{liq}$) − 14.9 ($X^{liq}_{CaO}X^{liq}_{SiO2}$) − 0.08ln ($X^{liq}_{TiO2}$) − 3.62 ln ($X^{liq}_{NaO_{0.5}}/X^{liq}_{KO_{0.5}}$) − 1.1 ($Mg\#^{iq}$) − 0.18ln ($X^{cpx}_{EnFs}$) − 0.027P] of Putirka et al. [13], which is a clinopyroxene-liquid geothermometer based on Jd-DiHd exchange and has been implemented with respect to the previous models of Putirka [14,15] through a larger experimental dataset and an increased number of regression parameters; the SEE for this geothermometer is 31.4 °C. For pressure estimates, we used Equation (32c) [P = −57.9 + 0.0745 T − 40.6($X^{liq}_{FeO}$) − 47.7($X^{cpx}_{CaTs}$) + 0.0676 ($H_2O^{liq}$) − 153($X^{liq}_{CaO_{0.5}}X^{liq}_{SiO_2}$) + 6.89($X^{cpx}_{Al}/X^{liq}_{AlO_{1.5}}$)] of Putirka et al. [13] which represents a geobarometer based on the partitioning of Al between clinopyroxene and liquid and whose SEE is 2.9 kbar. The estimated temperatures and pressures (Figure 11b) are reported in Table 3.

**Table 3.** Temperature and pressure output obtained from the Putirka [13] geothermobarometers applied to clinopyroxene-melt couples whose equilibrium has been verified with equilibrium test 1.

| Eruptive Period | Melt Composition | T (°C) | Average, s.d. | P (kbar) | Average, s.d. |
|---|---|---|---|---|---|
| Pre-CI | trachyte-phono-trachyte | 994–874 | 946 ± 34 | 10.6–3.4 | 6.2 ± 2 |
| CI | trachyte-phono-trachyte | 1015–894 | 953 ± 28 | 10–1.8 | 6.9 ± 1.6 |
| Pre-NYT | latite-trachyte | 1043–891 | 964 ± 42 | 12.5–3.8 | 8 ± 2.2 |
| NYT | trachyte-phono-trachyte | 1018–914 | 983 ± 23 | 9.2–3.3 | 6.9 ± 1.5 |
| Last 12 ka | shoshonite-latite- | 1110–884 | 976 ± 46 | 14.6–2.9 | 7.6 ± 2.1 |
| | trachyte-phono-trachyte | | | | |

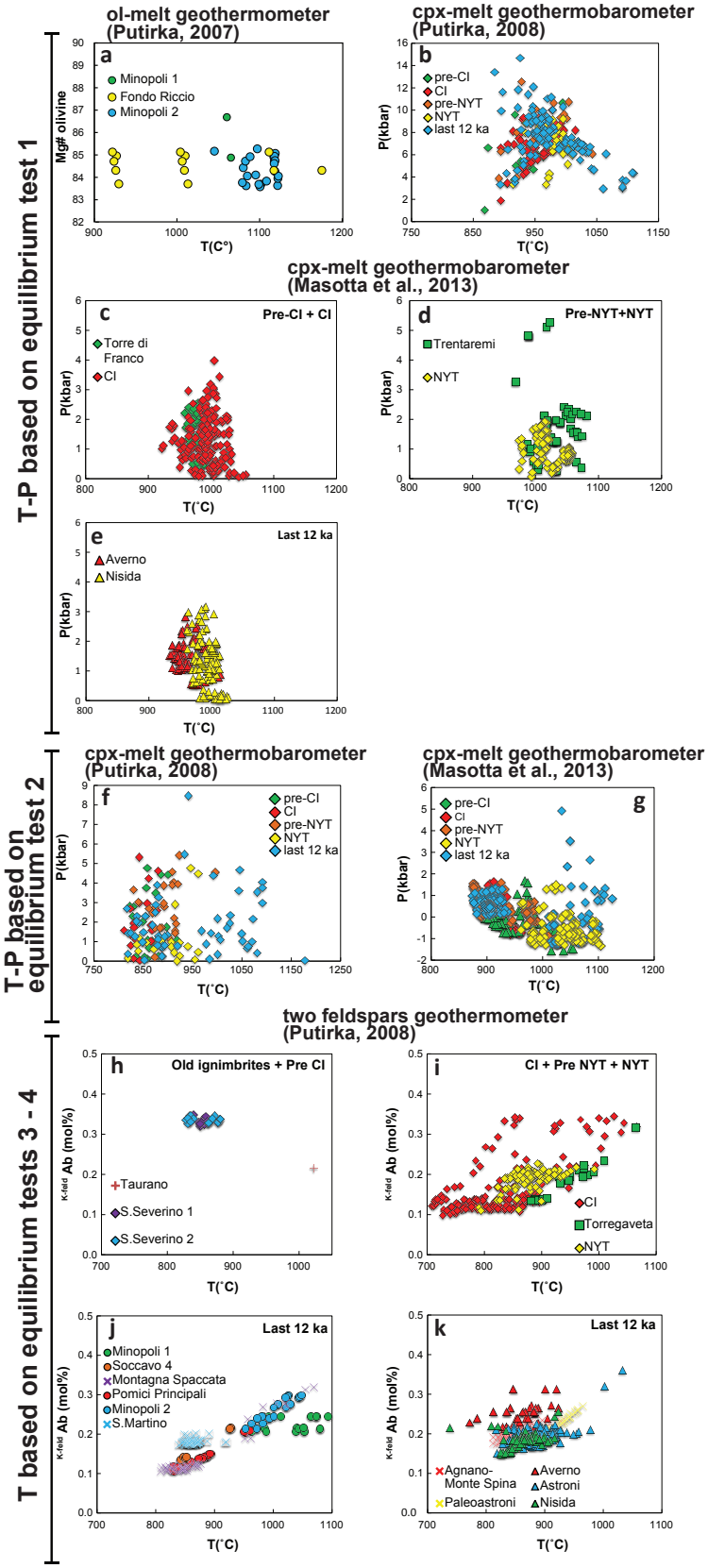


**Figure 11.** Temperature and pressure output results obtained for the Campi Flegrei minerals through the use of different combinations of geothermobarometric methods and equilibrium tests: (**a**) Mg# vs. T output of the olivine-melt geothermometer applied to olivine-melt couples whose equilibrium

has been tested with the equilibrium test 1; (**b**) T-P output of the clinopyroxene-melt geothermobarometer of Putirka [13] applied to clinopyroxene-melt couples whose equilibrium has been tested with the equilibrium test 1; (**c**–**e**) T-P output of the clinopyroxene-melt geothermobarometer of Masotta et al. [30] applied to clinopyroxene-melt couples whose equilibrium has been tested with the equilibrium test 1; (**f**) T-P output of the clinopyroxene-melt geothermobarometer of Putirka [13] applied to clinopyroxene-melt couples whose equilibrium has been tested with the equilibrium test 2; (**g**) T-P output of the clinopyroxene-melt geothermobarometer of Masotta et al. [30] applied to clinopyroxene-melt couples whose equilibrium has been tested with the equilibrium test 2; (**h**–**k**) $^{k\text{-feld}}$ Ab (mol %) vs. T output obtained from the two-feldspar geothermometer applied to plagioclase- and K-feldspar-melt couples resulted in equilibrium with equilibrium tests 3 and 4.

The geothermometer of Masotta et al. [30] was applied by using the equations Talk2012 [$10^4/T = 2.1 - 0.4 \ln (X^{cpx}_{Jd} X^{liq}_{Ca} X^{liq}_{FeO+MgO} / X^{cpx}_{DiHd} X^{liq}_{Na} X^{liq}_{Al}) + 0.038 (H_2O) - 1.64 (X^{liq}_{Mg}/X^{liq}_{Mg} + X^{liq}_{Fe}/X^{cpx}_{DiHd}) + 1.01 (X^{liq}_{Na}/X^{liq}_{Na} + X^{liq}_{K}) - 0.22 \ln (X^{liq}_{Ti}) + 0.47 \ln (X^{cpx}_{Jd}/X^{liq}_{Na} X^{liq}_{Al} (X^{cpx}_{Si})^2) + 1.62 (K_D{}^{liq\text{-}cpx}_{Fe\text{-}Mg}) + 23.39 (X^{liq}_{Ca} X^{liq}_{Si})$] and Palk2012 [$-3.89 + 0.38 (X^{cpx}_{Jd}/X^{liq}_{Na} X^{liq}_{Al} (X^{cpx}_{Si})^2) + 0.074 ((H_2O) + 5.01 (X^{liq}_{Na}/X^{liq}_{Na} + X^{liq}) + 6.39 (K_D{}^{liq\text{-}cpx}_{Fe\text{-}Mg})$], for estimating temperatures and pressures, respectively, which exhibit SEE lower than those of previous models ($SEE_{Talk2010}$ = 18.2 °C and $SEE_{Palk2012}$ = 1.15 kbar).

For each eruption, we plotted the T–P estimates obtained through this geothermobarometer specific for alkaline magmas (Figure 11c–e). The geothermobarometers of Masotta et al. [30] combine 10 clinopyroxene compositions with 10 melt compositions; in this case, we calculated P-T estimates only for a numerically appropriate set of data, i.e., only for those eruptions whose products have at least 10 mineral-melt couples in equilibrium. For example, for the pre-CI period, we applied geothermobarometry only to the Torre di Franco products (Figure 11c). Moreover, this geothermobarometer was used only for evolved compositions, since—as stated by Masotta et al. [30]—any attempt to use it on compositions different from those of their calibration dataset would produce high errors in estimation. The estimated temperatures and pressures are reported in Table 4.

**Table 4.** Temperature and pressure output obtained from the Masotta et al. [30] geothermobarometers applied to clinopyroxene-melt couples whose equilibrium has been verified with equilibrium test 1.

| Eruptive Period | Eruption | Melt Composition | T (°C) | Average, s.d. | P (kbar) | Average, s.d. |
|---|---|---|---|---|---|---|
| Pre-CI | Torre di Franco | trachyte | 994–958 | 978 ± 8 | 2.6–0.4 | 1.7 ± 0.6 |
| CI | CI | trachyte-phono-trachyte | 1055–921 | 992 ± 22 | 4.0–0.1 | 1.3 ± 0.8 |
| Pre-NYT | Trentaremi | trachyte | 1081–968 | 1025 ± 24 | 5.3–0.3 | 1.8 ± 1.14 |
| NYT | NYT | trachyte-phono-trachyte | 1058–973 | 1023 ± 22 | 1.9–0.1 | 1.0 ± 0.4 |
| Last 12 ka | Averno | trachyte-phono-trachyte | 1014–933 | 960 ± 16 | 2.8–0.5 | 1.6 ± 0.5 |
| | Nisida | trachyte-phono-trachyte | 1027–961 | 994 ± 15 | 3.2–0.1 | 1.3 ± 0.8 |

We also applied the same two geothermobarometers (Putirka, [13] and Masotta et al., [30]) to the clinopyroxene-melt couples that resulted in equilibrium through equilibrium test 2. When using Equations (33) and (32c) of the Putirka [13] geothermobarometer, a few clinopyroxene-melt couples yield negative values of the output pressures, which have not been taken into account. The estimated temperatures and pressures (Figure 11f) are reported in Table 5.

**Table 5.** Temperature and pressure output obtained from the Putirka [13] geothermobarometers applied to clinopyroxene-melt couples whose equilibrium has been verified with the equilibrium test 2.

| Eruptive Period | Rock Composition | T (°C) | Average, s.d. | P (kbar) | Average, s.d. |
|---|---|---|---|---|---|
| Pre-CI | trachyte-phono-trachyte | 918–823 | 946 ± 34 | 7.5–0.1 | 2.4 ± 2 |
| CI | trachyte-phono-trachyte | 886–811 | 848 ± 19 | 5.3–0.1 | 2.0 ± 1.4 |
| Pre-NYT | latite-trachyte | 996–830 | 892 ± 38 | 5.4–0.2 | 2.8 ± 2.3 |
| NYT | trachyte-phono-trachyte | 961–819 | 892 ± 42 | 4.8–0.1 | 2.2 ± 1.2 |
| Last 12 ka | shoshonite-latite- | 1179–817 | 946 ± 92 | 8.5–0.1 | 1.9 ± 1.5 |
| | trachyte-phono-trachyte | | | | |

When using the Talk2012 and Palk2012 equations of the Masotta et al. [30] geothermobarometers, most of the obtained pressures are negative, hence these values must be considered meaningless. In fact, the overall estimated pressures range from 4.9 to −1.6 kbar, with most of the values being <0 kbar (Figure 11g). The estimated temperatures and pressures are reported in Table 6.

**Table 6.** Temperature and pressure output obtained from the Masotta et al. [30] geothermobarometers applied to clinopyroxene-melt couples whose equilibrium has been verified with the equilibrium test 2.

| Eruptive Period | Rock Composition | T (°C) | Average-s.d. | P (kbar) |
|---|---|---|---|---|
| Pre-CI | trachyte-phono-trachyte | 1055–889 | 945 ± 43 | 1.9–(−1.6) |
| CI | trachyte-phono-trachyte | 963–900 | 934 ± 16 | 1.6–(−0.8) |
| Pre-NYT | trachyte | 1022–875 | 937 ± 47 | 1.6–(−0.9) |
| NYT | trachyte-phono-trachyte | 1105–961 | 1031 ± 31 | 1.5–(−1.3) |
| Last 12 ka | trachyte-phono-trachyte | 1125–875 | 953 ± 70 | 4.9–(−1.3) |

Lastly, Equation (27b) [$T = (-442 - 3.72P)/(-0.11 + 0.1\ln(X^{K\text{-feld}}{}_{Ab}/X^{pl}{}_{Ab}) - 3.27(X^{K\text{-feld}}{}_{An}) + 0.098(X^{K\text{-feld}}{}_{An}) + 0.52(X^{pl}{}_{An}\ X^{pl}{}_{Ab}))$] of the two-feldspar geothermometer of Putirka [13] was used on alkali feldspars and plagioclases resulting in equilibrium through tests 3 and 4, respectively. The estimated temperatures (Figure 11h,i) are reported in Table 7.

**Table 7.** Temperature output obtained from the two-feldspar geothermometer applied to plagioclase- and K-feldspar-melt couples resulted in equilibrium.

| Eruptive Period | Eruption | Melt Composition | T (°C) | Average, s.d. |
|---|---|---|---|---|
| Old ignimbrites | Taurano | - | 1193–1022 | 1071 ± 79 |
| Pre-CI | S.Severino 1 | trachyte | 879–833 | 855 ± 8 |
| | S.Severino 2 | trachyte | 880–828 | 853 ± 20 |
| CI | CI | trachyte-phono-trachyte | 1066–713 | 829 ± 70 |
| Pre-NYT | Torregaveta | latite | 1064–881 | 944 ± 45 |
| NYT | NYT | trachyte-phono-trachyte | 992–790 | 883 ± 30 |
| Last 12 ka | Minopoli 1 | shoshonite-latite | 1093–959 | 1035 ± 43 |

**Table 7.** *Cont.*

| Eruptive Period | Eruption | Melt Composition | T (°C) | Average, s.d. |
|---|---|---|---|---|
| | Pomici Principali | shoshonite-latite-trachyte | 959–826 | 870 ± 33 |
| | Soccavo 4 | trachyte | 928–842 | 871 ± 37 |
| | Minopoli 2 | shoshonite-trachyte | 1047–952 | 1007 ± 27 |
| | Montagna Spaccata | latite-trachyte | 1068–807 | 871 ± 67 |
| | S.Martino | trachyte | 920–839 | 864 ± 14 |
| | A-MS | trachyte-phono-trachyte | 928–812 | 857 ± 23 |
| | Paleoastroni 3 | trachyte | 964–905 | 930 ± 16 |
| | Averno | trachyte-phono-trachyte | 923–772 | 858 ± 30 |
| | Astroni | latite-trachyte | 1032–817 | 879 ± 29 |
| | Nisida | trachyte-phono-trachyte | 923–738 | 862 ± 21 |

## 5. Discussion

### *5.1. Magmatic Environments Reconstructed Based on Campi Flegrei Mineral Compositions*

Mineral compositions strongly depend on pre-eruptive (i.e., P-T) conditions in magma (e.g., [10,11,130]). Hence, crystals can preserve information about the set of parameters (pressure, temperature, oxygen fugacity and volatile content) of the environment where they formed. The chemical composition of the Campi Flegrei olivines, clinopyroxenes and feldspars show a polymodal distribution. This is evident in the forsterite (mol %) contents of olivines (Figure 3), in the Mg# of clinopyroxenes (Figure 4d), in the orthoclase (mol %) contents of alkali feldspars (Figure 6e) and in the anorthite (mol %) contents of plagioclases (Figure 6d). The occurrence of two main compositional populations detected in the Campi Flegrei minerals suggests two prevalent "magmatic environments" in which crystals have grown. A "magmatic environment" does not necessarily represent a physical environment and can be defined as a specific set of intensive thermodynamic variables (e.g., [131]) which determines the composition of a mineral. Among these two prevalent compositional populations, one, pertaining to olivines with $Fo_{90–88}$, clinopyroxenes with Mg# in the range 90–78, plagioclases with high anorthite content and K–feldspars with low orthoclase content, can be ascribed to mafic or poorly differentiated magmas; whereas the other, pertaining to clinopyroxenes with Mg# in the range 77–40 and K-feldspars with $Or_{88–68}$, can be associated with evolved magmas. The latter is the most abundant component and represents the typical magmatic environment in which minerals found in the Campi Flegrei trachytes and phonotrachytes form. The compositional bimodality occurs in the olivine, clinopyroxene and feldspar crystals from Campi Flegrei rocks emplaced over all the periods of activity, without significant differences. This suggests that through time, magmas formed reservoirs located at two different, barely constant depths in the Campi Flegrei plumbing system, where they stagnated/equilibrated. All the studied olivine, clinopyroxene and feldspar crystals show similar ranges of chemical variation over the different periods of activity. For clinopyroxene, the element variations (Figure 4) define continuous compositional trends that are consistent with fractional crystallization processes, responsible for most of the detected compositional variations. The element variation diagrams show a deviation in the correlation trends between Mg# and other elements, specifically when Mg# decreases below the 80 threshold. These deviations are likely due to the beginning of crystallization of other mineral phases that determines the different partition of elements into different phases. As an example, when feldspar begins

to crystallize together with the pre-existing clinopyroxene, the Al content of the melt is preferentially distributed in the feldspar. Furthermore, the $Al_2O_3$, $TiO_2$, $Na_2O$, $Cr_2O_3$ and MnO contents of clinopyroxenes from rocks belonging to the last 12 ka show different trends with respect to those of clinopyroxene from rocks of previous periods (Figure 4). In addition to the concomitance of crystallization of various phases, other processes able to determine the decoupling of elements should be considered. With respect to the previous periods, during the last 12 ka mafic magmas of deeper origin more frequently reached the upper crustal reservoirs. In fact, it is known that Mg-olivine-bearing (Section 4.1.1) mafic magmas (trachybasalt and latite) were erupted at Campi Flegrei only during the last period of activity, through vents located along a NE–SW regional fault system that probably tapped the deeper least-evolved reservoir (e.g., [66,110,120,132]). Diffusional modifications due to mixing between less and more evolved magmas can explain the observed different trends in the chemistry of minerals. The interaction between mafic and pre-existing evolved magmas or between melts and crystal mushes [94,133] would also explain part of the mineralogical disequilibria observed in the Campi Flegrei minerals (Figures 7–10). Open-system magmatic processes such as mixing/mingling (e.g., [94,98,101,110,134]), crustal contamination (e.g., [135]) and $CO_2$ flushing [88,101] have been hypothesized for the Campi Flegrei magmas, especially during the last 12 ka of activity. Such pre-eruptive processes could have decoupled earlier-grown crystals from their equilibrium melts. These findings are supported by the equilibrium tests themselves. In particular, in some of these (e.g., Figure 10), the linear and parabolic trends are possibly due to the occurrence of closed- and open-system processes, respectively. In fact, similarly, in addition to providing information on the possible occurrence of these processes, the $^{Fe\text{-}Mg}Kd_{min\text{-}liq}$ equilibrium test is also useful for the identification of xenocrysts and/or antecrysts, late crystallization, crystal removal and closed-system crystallization (e.g., [13,136]).

### *5.2. Reliability of the Equilibrium Tests for the Campi Flegrei Minerals*

For clinopyroxene, two different approaches (equilibrium test 1 and equilibrium test 2) were used here to test equilibrium between minerals and their melts. By applying equilibrium test 1 based on the Fe-Mg exchange coefficient to all the Campi Flegrei clinopyroxenes and screening all the mineral-melt pairs resulting in equilibrium (Figure 12a), we observe that almost all these couples are not in equilibrium, if they are tested by comparing the measured and predicted components (equilibrium test 2; Figure 12b).

Vice-versa, by applying this last method to the entire clinopyroxene-melt dataset and taking into account only clinopyroxene-melt couples in the 1:1 $\pm$ 0.05 line, it is possible to observe again a misfit with the method based on the $^{Fe\text{-}Mg}Kd_{cpx\text{-}liq}$ (Figure 12c,d).

The mismatch between the two tests can be explained in terms of the different parameters used in these methods. It is well-known that the equilibrium test based on the Fe–Mg exchange coefficient has certain limitations, and alone it is not sufficient to testify equilibrium crystallization: the $^{Fe\text{-}Mg}Kd_{min\text{-}liq}$ takes into account the behavior of the Fe-Mg exchange without considering that of minor elements, i.e., Al, Ca, Na, Ti, that can exhibit a wide range of variation in clinopyroxene (e.g., [13,126,137]). Putirka [13] showed that $^{Fe\text{-}Mg}Kd_{cpx\text{-}liq}$ is not a suitable tool for assessing equilibrium for a wide range of compositions. Similarly, the $^{Fe\text{-}Mg}Kd_{ol\text{-}liq}$ is sensitive to melt composition and hence fixed values for such coefficients cannot be applied (e.g., [138]). Therefore, an alternative and more suitable test for assessing equilibrium at the time of crystallization is based on the deviation of mineral components measured in a mineral such as clinopyroxene (Di, Hd, En, Fs, CaTs, CaTiTs, CaCrTs and Jd) from those predicted from the melt composition (e.g., [127]). Using this model, Putirka [13] and Mollo et al. [126,137] suggested that the difference between predicted and observed components provides a more robust test for equilibrium with respect to the method which takes into account the $^{Fe\text{-}Mg}Kd_{min\text{-}liq}$.

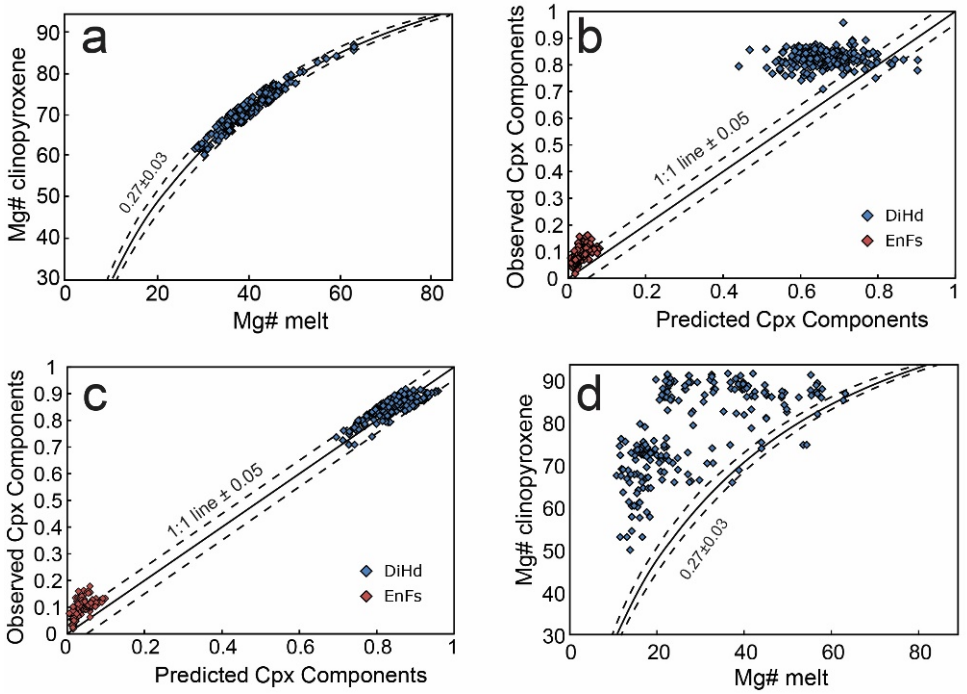


**Figure 12.** Comparison between the clinopyroxene-melt pairs resulted in equilibrium through test 1 and those resulted in equilibrium through test 2. The clinopyroxene-melt couples resulting in equilibrium through the Fe-Mg exchange coefficient (**a**) do not result in equilibrium comparing the measured and predicted DiHd component (**b**); the clinopyroxene-melt couples resulting in equilibrium through the comparison between measured and predicted DiHd component (**c**) do not result in equilibrium according to the Fe-Mg exchange coefficient (**d**).

In this regard, equilibrium test 2 represents a more adequate tool for the evaluation of equilibrium conditions. Nevertheless, the obtained pressure estimates on clinopyroxene-melt pairs resulting in equilibrium through this method cast some doubt on its reliability. In fact, for clinopyroxene-melt pairs whose equilibrium conditions have been verified by equilibrium test 2, negative values of the pressure estimates (Table 6) are obtained by applying the Equation (32c) of Putirka [13] and the Palk2012 of Masotta et al. [30]. This latter geobarometer has been chosen because it is specific for alkaline magmas and, in theory, more suitable for Campi Flegrei rocks; moreover, Equation (33) of Putirka [13] overestimates the temperature below 850 °C [30]. Still, a great number of negative pressure values have been obtained with the use of the Palk2012 equation. Such results raise doubts on the appropriateness of using this test for equilibrium coupled with the geothermobarometers of Masotta et al. [30]. On the other hand, both geobarometers, when applied to clinopyroxene-melt pairs in which the equilibrium has been verified through the $^{Fe\text{-}Mg}Kd_{cpx\text{-}liq}$, do not yield negative pressure estimates.

### *5.3. Reliability of the Temperatures Estimated for the Campi Flegrei Minerals*

A reliable magma temperature estimate goes beyond the information on how hot that magma was. The determination of temperature is critical, for example, in the application of diffusion modeling for timescale estimates. This allows for the retrieving of information on the residence times of crystals in subvolcanic plumbing systems with an important impact on the assessment of the current state of an active volcano during unrest (e.g., [57,139–143]). In particular, the obtained duration is exponentially dependent on the temperature value, since the latter is the crucial parameter used to calculate the diffusion coefficient (e.g., [144]).

For the temperature estimated through the geothermometers used in this work, regardless of the combination of equilibrium tests and geothermometer usage, the mineral-melt couples of the last 12 ka rocks always yield the widest temperature ranges. This is probably

due to the occurrence of rocks with poorly differentiated compositions besides those with evolved compositions, unlike previous periods (Figure 2).

In order to evaluate the robustness of the geothermometer–equilibrium test combinations, we compare the temperature output values obtained here with those estimated in previous studies. Forni et al. [55] estimated a pre-eruptive temperature for the CI in the range 1070–879 °C through the clinopyroxene-liquid geothermometers of Masotta et al. [30]. In previous works, the pre-eruptive temperatures of the CI magma were estimated in the range 980–800 °C, based on various methods: (i) comparing whole-rock compositions with the Nepheline (Ne)–Kalsilite (Ks)–Quartz (Qz) system [51,145]; (ii) two-feldspar geothermometry [51–53]; and (iii) homogenization temperatures of melt and fluid inclusions in clinopyroxene and K-feldspar [53]. The variable results obtained by different studies highlight the necessity to find a method allowing precise estimates of the temperatures for the Campi Flegrei minerals. Those obtained here for the CI are various, depending on the geothermometer used, the equilibrium test and combination thereof: the clinopyroxene-melt geothermometer of Putirka [13] based on equilibrium test 1 yielded temperatures in the range of 1015–894 °C; the geothermometer of Putirka [13] based on equilibrium test 2 yielded temperatures in the range of 886–811 °C; the geothermometer of Masotta et al. [30] based on equilibrium test 2 yielded temperatures in the range of 963–900 °C; the geothermometer of Masotta et al. [30] based on equilibrium test 1 yielded temperatures in the range 1055–921 °C; the two-feldspar geothermometry yielded temperatures in the range of 1076–713 °C. Compared to the previous estimates, the application of the clinopyroxene-melt geothermometers to mineral-melt couples whose equilibrium has been verified through the equilibrium test 2 narrows the temperature ranges. On the other hand, the two-feldspar geothermometer yields a wide range of temperatures. Nevertheless, it should be kept in mind that the equilibrium temperature of feldspars can be lower with respect to that of clinopyroxene, in the crystallization sequence. Regardless, the temperature ranges obtained with clinopyroxene-melt geothermometers based on equilibrium test 1 in this work are similar to those obtained in previous studies.

In Orsi et al. [83], at P of 1 kbar, the ternary-feldspar geothermometer [146] applied to the NYT magmas gave temperature estimates of 838–746 °C. More recently, Forni et al. [89] estimated a pre-eruptive temperature for the NYT magmas in the range of 1095–910 °C through the clinopyroxene-liquid geothermometers of Masotta et al. [30]. Even in this case, our results are different, depending on the used methods and combination thereof: the clinopyroxene-melt geothermometer of Putirka [13] based on equilibrium test 1 yielded temperatures in the range 1018–914 °C; the geothermometer of Putirka [13] based on equilibrium test 2 yielded temperatures in the range of 961–819 °C; the geothermometer of Masotta et al. [30] based on equilibrium test 2 yielded temperatures in the range 1105–961 °C; the geothermometer of Masotta et al. [30] based on equilibrium test 1 yielded temperatures in the range of 1058–973 °C; the two-feldspar geothermometer yielded temperatures in the range of 992–790 °C. Hence, even in this case, the temperature ranges that most match the literature estimates are those obtained by geothermometers applied to mineral-melt couples whose equilibrium has been verified through equilibrium test 1.

For the Agnano–Monte Spina eruption trachytes, temperatures are constrained by both experimental petrology [54] and two-feldspar geothermometry [57] between 973 and 870 °C. In this work, no Agnano–Monte Spina clinopyroxene-melt couple passed equilibrium test 2. Hence, our estimates for pre-eruptive temperatures come from the clinopyroxene-melt geothermometer [13] applied to clinopyroxene-melt couples whose equilibrium has been verified with the $^{Fe\text{-}Mg}Kd_{cpx\text{-}liq}$ and from the two-feldspar geothermometer: the temperatures estimated with these geothermometers are in the ranges of 946–893 °C and 928–812 °C, respectively. The former estimates are in agreement with those of previous works, whereas the latter only partly fit. However, our results are more robust because we used a greater amount of data with respect to those of previous studies, in which the equilibrium conditions were not verified before applying geothermometry.

Astbury et al. [58] applied the Masotta et al. [30] geothermobarometers to clinopyroxene crystals of the Astroni eruption and obtained temperatures in the range of 980–960 °C and pressures in the range of 2.2–0.2 kbar. They also applied two-feldspar geothermometry (Equation (27); [13]) to feldspar rims that gave temperatures ranging from 970 to 800 °C. Here, we obtained T–P estimates for the Astroni eruption through the Putirka [13] clinopyroxene-melt geothermobarometers. The latter method, when applied to mineral-melt couples which passed equilibrium test 1, yielded temperatures in the range of 981–884 °C and pressures in the range of 13.4–5.8 kbar, while when applied to mineral-melt couples resulted in equilibrium via test 2 yielded temperatures in the range of 919–830 °C and pressures in the range of 1.4–0.7 kbar. The estimated T partially match the values obtained by Astbury et al. [58]. Nevertheless, the pressures obtained with the Putirka [13] geobarometer applied to mineral-melt couples that resulted in equilibrium via test 1 are unrealistically high (13.4–5.8 kbar).

D'Oriano et al. [116], Piochi et al. [95] and Arzilli et al. [47], based on phase relations and geothermometry, estimated that in the magma(s) feeding the Monte Nuovo eruption, phenocrysts formed at equilibrium temperatures of ~890–800 °C, whereas the microlite equilibrium temperatures were even higher (~1100–900 °C). Since no clinopyroxene-melt couple of Monte Nuovo rocks passed equilibrium test 1, our temperature estimates come from the two clinopyroxene-melt geothermometers applied to mineral-melt couples whose equilibrium has been verified through test 2. In particular, the Putirka [13] geothermometer yielded temperatures in the range of 899–834 °C and the Masotta et al. [30] geothermometer yielded temperatures in the range of 911–895 °C. Since our estimates are based on phenocrysts only, we can observe a good fit of the temperature values obtained through the Putirka [13] geothermometer with those of the literature.

### *5.4. Reliability of Pressures Estimated for Campi Flegrei Minerals*

Calculated pressures together with bedrock density allow for the estimation of depths of crystallization, and hence, potential magma storage depth. Determining magma storage depths is essential for various reasons. For example, understanding the distribution of magma storage depths is important for linking magmatic processes to the expressions of ongoing unrest such as seismicity, ground deformation and gas emission, especially in volcanically active areas [147–149], as well as to provide information about mechanisms of crustal formation [150–152].

Regarding pressure estimates, in order to evaluate the reliability of the different equilibrium test–geobarometer couples used here, we compare our results with those obtained with different methods used in literature (e.g., geophysical investigations, melt inclusions, phase equilibria) to infer the storage depth of Campi Flegrei magmas. In recent decades, geochemical and geophysical investigations allowed for the assessment that the Campi Flegrei plumbing system is characterized by deep and shallow reservoirs, [31–34,36–45,47,49,87,88,95,101,121,132,135,153–162]. However, although the detachment of magma at a depth $\geq$ 8 km is widely accepted, there is no consensus about the structure of the plumbing system at shallower levels. In fact, some authors hypothesized the presence of permanent small magma chambers feeding the last 5000 years of activity, including the last event, at ~4–1 km of depth (Monte Nuovo eruption; [48,58,163]), while other authors suggested the development of an ephemeral localized storage zone during the magma ascent, where magma shortly resides until erupting or cooling (the so-called failed eruptions, e.g., [97]).

Regarding the large-volume CI eruption, Fabbrizio and Carroll [35] estimated that the magma reservoir was stored between 5 and 8 km below the surface, through experimental constraints on phase relations. Using thermodynamic modeling, Bohrson et al. [164] revealed that in the magmas feeding the CI eruption, major element variations were dominated by crystal–liquid separation at pressures corresponding to ~7–5 km. Melt inclusions in crystals from CI analyzed by Marianelli et al. [117] yield a relatively wide range of pressure for the magmatic storage and degassing located at 2–6 km depth. Sim-

ilarly, the phase-equilibria calculations performed by Fowler et al. [118] on CI glass and mineral compositions indicate isobaric fractionation at 0.15 GPa (∼6 km depth). Pappalardo et al. [72], using geochemical and textural analyses, suggested that a wide sill-like trachytic magma chamber was active under the Campanian Plain at ca 2.5 kbar before CI eruption. Fanara et al. [46], through a combination of natural and experimental data, proved that the CI magma could have been stored or ponded during its rising path at two different levels: a deeper one corresponding to a depth of about 8 to 15 km and a shallower one at about 1 to 8 km. Moretti et al. [165], through melt-inclusion-based studies of gas-melt saturation, pointed out that the huge volume of magma that extruded during the CI eruption differentiated and mixed at ∼6–3 km.

Hence, several studies provided different estimates of the storage conditions for the Campi Flegrei magmas that are also very variable for the same case study (e.g., the CI eruption). In most of these studies, the main inferred estimates range between ∼12 and ∼4 km, corresponding to a pressure range of ∼3–1 kbar, using a crustal density of 2.6 g/cm$^3$ according to Berrino et al. [166]. This estimate is not precise and there is no possibility to really discriminate among two or more main magma storage depths, considering the SEE of the geobarometers. However, this pressure range seems reasonable since the anomalous layer with the shape of a wide sill extending below the Campi Flegrei area at ∼11–7 km depth identified in different geophysical studies (e.g., [31–34,36–38]) is generally accepted as the main storage region of Campi Flegrei magmas. By considering the wide range of pressures (~14.7–1 kbar) obtained with the Putirka [13] geobarometer based on equilibrium test 1, we cannot consider it as a good method for estimating the crystallization pressures of Campi Flegrei magmas. In fact, the most frequent pressure value obtained with this method is ∼7.5 kbar (Figure 13a), which corresponds to a depth of ∼29 km, by using a crustal density of 2.6 g/cm$^3$, which is quite unreasonable for evolved magmas.

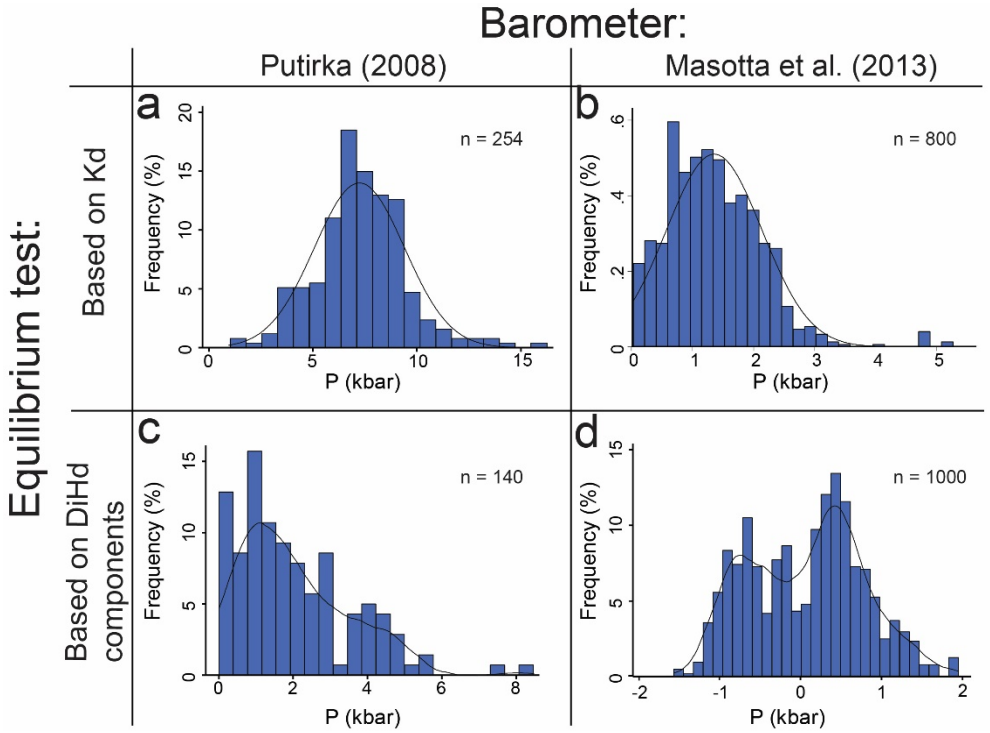


**Figure 13.** Comparison of the estimated pressures (kbar) obtained through the various methods combining equilibrium tests and geobarometers; (**a**) frequency (%) histogram of pressure estimates obtained through the equation 32c of the Putirka [13] geobarometer applied to clinopyroxene-melt couples whose equilibrium has been verified with equilibrium test 1; (**b**) frequency (%) histogram of pressure estimates obtained through the equation Palk2012 of the Masotta et al. [30] geobarometer

applied to clinopyroxene-melt couples whose equilibrium has been verified with equilibrium test 1; (**c**) frequency (%) histogram of pressure estimates obtained through the equation 32c of the Putirka [13] geobarometer applied to clinopyroxene-melt couples whose equilibrium has been verified with equilibrium test 2; (**d**) frequency (%) histogram of pressure estimates obtained through the equation Palk2012 of the Masotta et al. [30] geobarometer applied to clinopyroxene-melt couples whose equilibrium has been verified with equilibrium test 2.

Equation (32c) of Putirka [13] applied to clinopyroxene-melt couples resulting in equilibrium with test 2 yields estimates that are more in agreement with those obtained in the literature. In this case, the pressures range from ∼5.6 to 0.1 kbar, with two outsider values at 8.4 and 7.5 kbar (Figure 13c). The pressure values show a bimodal distribution characterized by two main peaks at 1.5 kbar and 4.1 kbar. These values correspond to depths of ∼6 km and 16 km, by using a crustal density of 2.6 g/cm$^3$. The first value is in agreement with depths of shallow reservoirs (≤8 km) frequently estimated in previous studies. The second value could be attributed to region of magma storage below 8 km depth. Nevertheless, it should keep in mind that precise depth estimates can be under- or over-estimated for the uncertainty due to the lack of reliable data on the average density of rocks at various depths (km).

### *5.5. Reliability of the Different Geothermobarometers Based on Different Equilibrium Tests for the Campi Flegrei Minerals*

Based on the comparison with T–P estimates published in the literature, we can evaluate which combination of geothermobarometer–equilibrium test can be most suitable for the Campi Flegrei magmas. For temperatures, the two-feldspar geothermometer yields values commonly slightly lower compared to those obtained in the literature through independent studies. Overall, the geothermometers applied to clinopyroxene-melt couples whose equilibrium has been tested through test 2 do not yield temperature values fitting those estimated in previous works. On the other hand, the geothermometer of Putirka [13] applied to clinopyroxene-melt couples whose equilibrium has been tested through the Kd can be considered the most reliable combination of methods, being able to match the pre-eruptive temperature values obtained in previous studies. This finding is valid for all the eruptions fed by compositionally heterogeneous magmas, such as CI, NYT, Agnano-Monte Spina and Astroni 6, which show evidence of pre-eruptive interaction between less- and more-differentiated magmas (e.g., [55,56,59,83,88,91,94,98,101,120]). For magmas showing homogeneous and highly differentiated compositions (e.g., Monte Nuovo), the clinopyroxene-melt geothermometers applied to mineral-melt couples whose equilibrium has been verified through equilibrium test 2 can be considered the most adequate tool for the estimation of temperatures.

For the pressure estimates, as previously shown, when coupled with the equilibrium test 2, the geobarometer of Masotta et al. [30] yields a great number of negative output pressures. The most reliable pressure estimates, not affected by negative values and reasonable being comparable to those obtained through independent studies, are those obtained with the geobarometer specific for alkaline magmas [30] applied to clinopyroxenes-melt couples, whose equilibria have been verified with test 1. However, this geobarometer was calibrated on a set of experimental data at low pressures; this allows for the investigation of crystallization depths only in the shallower part of the Campi Flegrei magmatic system, casting doubts on depth estimates of its deeper portion. In this regard, the use of such a geobarometer can be an efficient tool for estimating crystallization pressures of minerals in shallow reservoirs and for obtaining useful information about syn-eruptive conditions (magma degassing, magma rising velocity, e.g., through study of microliths, crystal size distribution, etc.), but it does not give the possibility to investigate processes occurring at high depths.

## 6. Conclusions

Most of the findings which are discussed are based on the comparison between our geothermobarometric estimates and those obtained in other works through different methods, i.e., melt inclusion and phase relation studies. However, it is largely demonstrated that melt-inclusion data can be affected by post-entrapment modification, as well as that the inclusion-bearing crystals can have a wide range of origins and ages, further complicating the interpretation of magmatic processes [167]. Thus, melt inclusions' volatile contents do not univocally record pre-eruptive storage depth but can follow syn-eruption degassing paths.

The mineral chemistry of the Campi Flegrei olivine, clinopyroxene and feldspar is characterized by two main compositional populations that are recurrent over all the periods of activity. Moreover, the chemical variation trend detected in minerals belonging to the last 12 ka and their numerous mineral-melt disequilibria testify, during this period, to a frequent occurrence of open-system processes (mingling/mixing, crustal assimilation, $CO_2$ flushing) able to produce diffusive effects and to decouple crystals from their equilibrium melts. Nevertheless, such prevalent compositions suggest that two main sets of thermodynamic variables (T, P) rule the growth of crystals and, hence, the storage conditions of the Campi Flegrei magmas. These two magmatic environments can be ascribed to mafic and evolved magmas, which presumably characterize deep and shallow reservoirs, respectively. Nevertheless, the current geothermobarometric methods do not allow precisely constraining and distinguishing the depth and temperature of the two main magmatic environments. Interestingly, the combination of equilibrium tests considered less robust with geothermobarometric methods considered less appropriate for the Campi Flegrei magma compositions yields estimates that are in agreement with results obtained in independent studies. In fact, our results highlight that (i) there is a low reliability for the combinations of the most recent equilibrium tests and geothermometric and geobarometric methods, which theoretically are the most suitable for the Campi Flegrei alkaline magmas; (ii) although equilibrium test 1 has certain theoretical limitations and is considered less suitable than equilibrium test 2, the mineral-melt couples resulting in equilibrium with the former test produced geothermobarometric estimates that are more in agreement with previous work estimates; (iii) the right choice for the best approximation of the geothermometric and geobarometric estimates depends, case by case, on the compositional features of the erupted products. In fact, the occurrence of frequent open-system magmatic processes, which influenced the chemical-physical conditions (temperature, volatile content, etc.) of the plumbing system, makes the application of classic geothermobarometric approaches critical.

From all these considerations, it is clearly possible to obtain information on the architecture of the Campi Flegrei magmatic system from the geothermobarometric estimates, but the critical issues highlighted in this work suggest that in complex systems such as the Campi Flegrei one, the application of combined methods must be preferred over the single approach.

**Supplementary Materials:** The following are available online at https://www.mdpi.com/article/10.3390/min12030308/s1, Table S1: Major and minor element contents of olivine, clinopyroxene and feldspar crystals from investigated rocks.

**Author Contributions:** C.P. and M.D. defined the study; L.P., M.D. and I.A. provided the samples; M.D., L.P., V.D.R. and C.P. performed EMP analyses; C.P. wrote the original draft and performed data analysis; C.P., R.S.I., P.P. and M.D. dealt with the visualization and presentation of data; investigation, interpretation and writing—review and editing were carried out by all authors. All authors have read and agreed to the published version of the manuscript.

**Funding:** This research partially benefited from funding provided by the Italian Presidenza del Consiglio dei Ministri-Dipartimento della Protezione Civile (DPC, DPC-INGV V2 project). Scientific papers funded by the DPC do not represent its official opinions and policies. The INGV, OV laboratories have been also financially supported by the EPOS Research Infrastructure through the contribution of the Italian Ministry of University and Research (MUR).

**Data Availability Statement:** The data presented in this study are partly available in Supplementary Materials; all other data are available on request from the corresponding author.

**Acknowledgments:** Andrea Cavallo and Manuela Nazzari are thanked for their assistance during analytical sessions at HP-HT Laboratory of Experimental Volcanology and Geophysics of the Istituto Nazionale di Geofisica e Vulcanologia in Rome (Italy). The manuscript benefitted from the constructive comments by three anonymous reviewers.

**Conflicts of Interest:** The authors declare no conflict of interest.

## References

1. Eichelberger, J.C. Vesiculation of mafic magma during replenishment of silicic magma reservoirs. *Nature* **1980**, *288*, 446–450. [CrossRef]
2. Anderson, A.T. Probable relations between plagioclase zoning and magma dynamics, Fuego volcano, Guatemala. *Am. Min.* **1984**, *69*, 660–676.
3. Helz, R.T. Diverse olivine types in lavas of the 1959 eruption of Kilauea volcano and their bearing on eruption dynamics. In *Volcanism at Hawaii*; Geological Survey Professional Paper; Decker, R.W., Wright, T.L., Stauffer, P.H., Eds.; United States Government Printing Office: Washington, DC, USA, 1987; Volume 1350, pp. 691–722.
4. Hibbard, M.J. The magma mixing origin of mantled feldspars. *Contrib. Mineral. Petrol.* **1981**, *76*, 158–170. [CrossRef]
5. Humphreys, M.C.S.; Blundy, J.D.; Sparks, R.S.J. Magma evolution and open-system processes at Shiveluch volcano: Insights from phenocryst zoning. *J. Petrol.* **2006**, *47*, 2303–2334. [CrossRef]
6. Singer, B.S.; Dungan, M.A.; Layne, G.D. Textures and Sr, Ba, Mg, Fe, K, and Ti compositional profiles in volcanic plagioclase: Clues to the dynamics of calc-alkaline magma chambers. *Amer. Min.* **1995**, *80*, 776–798. [CrossRef]
7. Wallace, G.S.; Bergantz, G.W. Wavelet-based correlation (WBC) of zoned crystal populations and magma mixing. *Earth Planet Sci. Lett.* **2002**, *202*, 133–145. [CrossRef]
8. Wallace, G.S.; Bergantz, G.W. Constraints on mingling of crystal populations from off-center zoning profiles: A statistical approach. *Am. Min.* **2004**, *89*, 64–73. [CrossRef]
9. Wallace, G.S.; Bergantz, G.W. Reconciling heterogeneity in crystal zoning data: An application of shared characteristic diagrams at Chaos Crags, Lassen Volcanic Center California. *Contrib. Mineral. Petrol.* **2005**, *149*, 98–112. [CrossRef]
10. Ginibre, C.; Wörner, G.; Kronz, A. Crystal zoning as an archive for magma evolution. *Elements* **2007**, *3*, 261–266. [CrossRef]
11. Streck, M.J. Mineral textures and zoning as evidence for open system processes. *Rev. Mineral. Geochem.* **2008**, *69*, 595–622. [CrossRef]
12. Powell, R.; Holland, T. Optimal geothermometry and geobarometry. *Am. Mineral.* **1994**, *79*, 120–133.
13. Putirka, K.D. Thermometers and barometers for volcanic systems. *Rev. Mineral. Geochem.* **2008**, *69*, 61–120. [CrossRef]
14. Putirka, K.D.; Johnson, M.; Kinzler, R.J.; Longhi, J.; Walker, D. Thermobarometry of mafic igneous rocks based on clinopyroxene-liquid equilibria, 0–30 kbar. *Contrib. Mineral. Petrol.* **1996**, *123*, 92–108. [CrossRef]
15. Putirka, K.D.; Mikaelian, H.; Ryerson, F.; Shaw, H. New clinopyroxene– liquid thermobarometers for mafic, evolved, and volatile-bearing lava compositions, with applications to lavas from Tibet and the Snake River Plain, Idaho. *Am. Min.* **2003**, *88*, 1542–1554. [CrossRef]
16. Neave, D.A.; Putirka, K.D. A new clinopyroxene-liquid barometer, and implications for magma storage pressures under Icelandic rift zones. *Am. Min.* **2017**, *102*, 777–794. [CrossRef]
17. Johnson, M.C.; Rutherford, M.J. Experimental calibration of the aluminium- in-hornblende geobarometer with application to Long Valley caldera (California) volcanic rocks. *Geology* **1989**, *17*, 837–841. [CrossRef]
18. Henry, D.J.; Guidotti, C.V.; Thomson, J.A. The Ti-saturation surface for low-to-medium pressure metapelitic biotites: Implications for geothermometry and Ti-substitution mechanisms. *Am. Min.* **2005**, *90*, 316–328. [CrossRef]
19. Nimis, P. A clinopyroxene geobarometer for basaltic systems based on crystal-structure modeling. *Contrib. Mineral. Petrol.* **1995**, *121*, 115–125. [CrossRef]
20. Nimis, P. Clinopyroxene geobarometry of magmatic rocks. Part 2. Structural geobarometers for basic to acid, tholeiitic and mildly alkaline magmatic systems. *Contrib. Mineral. Petrol.* **1999**, *135*, 62–74. [CrossRef]
21. Nimis, P.; Ulmer, P. Clinopyroxene geobarometry of magmatic rocks. Part 1. An expanded structural geobarometer for anhydrous and hydrous basic and ultrabasic systems. *Contrib. Mineral. Petrol.* **1998**, *133*, 122–135. [CrossRef]
22. Yang, H.J.; Kinzler, R.J.; Grove, T. Experiments and models of anhydrous, basaltic olivine plagioclase-augite saturated melts from 0.001 to 10 kbar. *Contrib. Mineral. Petrol.* **1996**, *124*, 1–18. [CrossRef]
23. Benisek, A.; Kroll, H.; Cemic, L. New developments in two-feldspar thermometry. *Am. Min.* **2004**, *89*, 1496–1504. [CrossRef]
24. Bali, E.; Hartley, M.; Halldórsson, S.; Gudfinnsson, G.; Jakobsson, S. Melt inclusion constraints on volatile systematics and degassing history of the 2014–2015 Holuhraun eruption, Iceland. *Contrib. Mineral. Petrol.* **2018**, *173*, 9. [CrossRef]
25. Kroll, H.; Evangelakakis, C.; Voll, G. Two-feldspar geothermometry: A review and revision for slowly cooled rocks. *Contrib. Mineral. Petrol.* **1993**, *114*, 510–518. [CrossRef]
26. Lindsley, D.H.; Andersen, D.J. A two-pyroxene thermometer. *J. Geophys. Res.* **1983**, *88*, 887–890. [CrossRef]

27. Putirka, K.D. Geothermometry and Geobarometry. In *Encyclopedia of Geochemistry: A Comprehensive Reference Source on the Chemistry of the Earth*; White, W.M., Ed.; Springer International Publishing: Cham, Switzerland, 2018; pp. 597–614.
28. Putirka, K.D. Igneous thermometers and barometers based on plagioclase + liquid equilibria: Tests of some existing models and new calibrations. *Am. Min.* **2005**, *90*, 336–346. [CrossRef]
29. Giacomoni, P.P.; Coltorti, M.; Bryce, J.G.; Fahnestock, M.F.; Guitreau, M. Mt. Etna plumbing system revealed by combined textural, compositional, and thermobarometric studies in clinopyroxenes. *Contrib. Mineral. Petrol.* **2016**, *171*, 34. [CrossRef]
30. Masotta, M.; Mollo, S.; Freda, C.; Gaeta, M.; Moore, G. Clinopyroxene–liquid thermometers and barometers specificto alkaline differentiated magmas. *Contrib. Mineral. Petrol.* **2013**, *166*, 1545–1561. [CrossRef]
31. Zollo, A.; Gasparini, P.; Virieux, J.; le Meur, H.; de Natale, G.; Biella, G.; Boschi, E.; Capuano, P.; de Franco, R.; dell'Aversana, P.; et al. Seismic evidence for a low-velocity zone in the upper crust beneath Mount Vesuvius. *Science* **1996**, *274*, 592–594. [CrossRef]
32. Zollo, A.; Maercklin, N.; Vassallo, M.; Dello Iacono, D.; Virieux, J.; Gasparini, P. Seismic reflections reveal a massive melt layer feeding Campi Flegrei caldera. *Geophys. Res. Lett.* **2008**, *35*, L12306. [CrossRef]
33. De Natale, G.; Troise, C.; Pingue, F. A mechanical fluid-dynamical model for ground movements at Campi Flegrei caldera. *J. Geodyn.* **2001**, *32*, 487–517. [CrossRef]
34. De Natale, G.; Troise, C.; Pingue, F.; Mastrolorenzo, G.; Pappalardo, L.; Battaglia, M.; Boschi, E. The Campi Flegrei caldera: Unrest mechanisms and hazard. *Geol. Soc. Spec. Publ.* **2006**, *269*, 25–45. [CrossRef]
35. Fabbrizio, A.; Carroll, M.R. Experimental constraints on the differentiation process and pre-eruptive conditions in the magmatic system of Phlegrean fields (Naples, Italy). *J. Volcanol. Geotherm. Res.* **2008**, *171*, 88–102. [CrossRef]
36. Guidarelli, M.; Zille, A.; Saraò, A.; Natale, M.; Nunziata, C.; Panza, G.F. Shear-wave velocity models and seismic sources in campanian volcanic areas: Vesuvius and Phlegraean fields. In *Vesuvius: Education, Security and Prosperity*; Dobran, F., Ed.; Elsevier: Amsterdam, The Netherlands, 2006; Volume 8, pp. 287–309.
37. Nunziata, C.; Natale, M.; Luongo, G.; Panza, G.F. Magma reservoir at Mt. Vesuvius: Size of the hot, partially molten, crust material detected deeper than 8 km. *Earth Planet. Sci. Lett.* **2006**, *242*, 51–57. [CrossRef]
38. Nunziata, C. Low shear-velocity zone in the Neapolitan-area crust between the Campi Flegrei and Vesuvio volcanic areas. *Terra Nova* **2010**, *22*, 208–217. [CrossRef]
39. De Siena, L.; Del Pezzo, E.; Bianco, F. Seismic attenuation imaging of Campi Flegrei: Evidence of gas reservoirs, hydrothermal basins, and feeding systems. *J. Geophys. Res.* **2010**, *115*, B09312. [CrossRef]
40. Woo, J.Y.; Kilburn, C.R. Intrusion and deformation at Campi Flegrei, southern Italy: Sills, dikes, and regional extension. *J. Geophys. Res.* **2010**, *115*. [CrossRef]
41. Costanzo, M.R.; Nunziata, C. Lithospheric Vs models in the Campanian Plain (Italy) by integrating Rayleigh wave dispersion data from noise cross correlation functions and earthquake recordings. *Phys. Earth Planet. Inter.* **2014**, *234*, 46–59. [CrossRef]
42. Costanzo, M.R.; Nunziata, C. Inferences on the lithospheric structure of Campi Flegrei District (Southern Italy) from seismic noise cross-correlation. *Phys. Earth Planet. Inter.* **2017**, *265*, 92–105. [CrossRef]
43. Amoruso, A.; Crescentini, L.; Sabbetta, I.; De Martino, P.; Obrizzo, F.; Tammaro, U. Clues to the cause of the 2011–2013 Campi Flegrei caldera unrest, Italy, from continuous GPS data. *Geophys. Res. Lett.* **2014**, *42*, 3847–3854. [CrossRef]
44. D'Auria, L.; Pepe, S.; Castaldo, R.; Giudicepietro, F.; Macedonio, G.; Ricciolino, P.; Tizzani, P.; Casu, F.; Lanari, R.; Manzo, M.; et al. Magma injection beneath the urban area of Naples: A new mechanism for the 2012–2013 volcanic unrest at Campi Flegrei caldera. *Sci. Rep.* **2015**, *5*, 13100. [CrossRef]
45. Di Maio, R.; Piegari, E.; Mancini, C.; Scandone, R. Numerical study of conductive heat losses from a magmatic source at Phlegraean Fields. *J. Volcanol. Geotherm. Res.* **2015**, *290*, 75–81. [CrossRef]
46. Fanara, S.; Botcharnikov, R.E.; Palladino, D.M.; Adams, F.; Buddensieck, J.; Mulch, A.; Behrens, H. Volatiles in magmas related to the Campanian ignimbrite eruption: Experiments vs. natural findings. *Am. Mineral.* **2015**, *100*, 2284–2297. [CrossRef]
47. Arzilli, F.; Piochi, M.; Mormone, A.; Agostini, C.; Carroll, M.R. Constraining pre-eruptive magma conditions and unrest timescales during the Monte Nuovo eruption (1538 AD.; Campi Flegrei, Southern Italy): Integrating textural and CSD results from experimental and natural trachy-phonolites. *Bull. Volcanol.* **2016**, *78*, 72. [CrossRef]
48. Di Vito, M.A.; Acocella, V.; Aiello, G.; Barra, D.; Battaglia, M.; Carandente, A.; Del Gaudio, C.; de Vita, S.; Ricciardi, G.P.; Ricco, C.; et al. Magma transfer at Campi Flegrei caldera (Italy) before the 1538 AD eruption. *Sci. Rep.* **2016**, *6*, 32245. [CrossRef]
49. Fedi, M.; Cella, F.; D'Antonio, M.; Florio, G.; Paoletti, V.; Morra, V. Gravity modeling finds a large magma body in the deep crust below the Gulf of Naples, Italy. *Sci. Rep.* **2018**, *8*, 8229. [CrossRef]
50. Pappalardo, L.; Buono, G. Insights into Processes and Timescales of Magma Storage and Ascent from Textural and Geochemical Investigations: Case Studies from High-Risk Neapolitan Volcanoes (Italy). In *Crustal Magmatic System Evolution: Anatomy, Architecture, and Physico-Chemical Processes*; Masotta, M., Beier, C., Mollo, S., Eds.; John Wiley & Sons: Hoboken, NJ, USA, 2021; pp. 213–235.
51. Melluso, L.; Morra, V.; Perrotta, A.; Scarpati, C.; Adabbo, M. The eruption of the Breccia Museo (Campi Flegrei, Italy): Fractional crystallization processes in a shallow, zoned magma chamber and implications for the eruptive dynamics. *J. Volcanol. Geotherm. Res.* **1995**, *68*, 325–339. [CrossRef]
52. Civetta, L.; Orsi, G.; Pappalardo, L.; Fisher, R.V.; Heiken, G.; Ort, M. Geochemical zoning, mingling, eruptive dynamics and depositional processes—The Campanian Ignimbrite, Campi Flegrei caldera, Italy. *J. Volcanol. Geotherm. Res.* **1997**, *75*, 183–219. [CrossRef]

53. Fulignati, P.; Marianelli, M.; Proto, M.; Sbrana, A. Evidences for disruption of a crystallizing front in a magma chamber during caldera collapse: An example from the Breccia Museo unit (Campanian Ignimbrite eruption, Italy). *J. Volcanol. Geotherm. Res.* **2004**, *133*, 141–155. [CrossRef]
54. Roach, A.L. The Evolution of Silicic Magmatism in the Post-Caldera Volcanism of the Phlegrean Fields, Italy. Ph.D. Thesis, Brown University, Providence, RI, USA, 2005.
55. Forni, F.; Bachmann, O.; Mollo, S.; De Astis, G.; Gelman, S.E.; Ellis, B.S. The origin of a zoned ignimbrite: Insights into the Campanian Ignimbrite magma chamber (Campi Flegrei, Italy). *Earth Planet. Sci. Lett.* **2016**, *449*, 259–271. [CrossRef]
56. Forni, F.; Petricca, E.; Bachmann, O.; Mollo, S.; De Astis, G.; Piochi, M. The role of magma mixing/mingling and cumulate melting in the Neapolitan Yellow Tuff caldera-forming eruption (Campi Flegrei, Southern Italy). *Contrib. Mineral. Petrol.* **2018**, *173*, 45. [CrossRef]
57. Iovine, R.S.; Fedele, L.; Mazzeo, F.C.; Arienzo, I.; Cavallo, A.; Wörner, G.; Orsi, G.; Civetta, L.; D'Antonio, M. Timescales of magmatic processes occurred prior to the ca 47 ka Agnano-Monte Spina eruption (Campi Flegrei caldera Southern Italy) based on diffusion chronometry on sanidine phenocrysts. *Bull. Volcanol.* **2017**, *79*, 18. [CrossRef]
58. Astbury, R.L.; Petrelli, M.; Ubide, T.; Stock, M.J.; Arienzo, I.; D'Antonio, M.; Perugini, D. Tracking plumbing system dynamics at the Campi Flegrei caldera Italy: High-resolution trace element mapping of the Astroni crystal cargo. *Lithos* **2018**, *318–319*, 464–477. [CrossRef]
59. Gebauer, S.K.; Schmitt, A.K.; Pappalardo, L.; Stockli, D.F.; Lovera, O.M. Crystallization and eruption ages of Breccia Museo (Campi Flegrei caldera, Italy) plutonic clasts and their relation to the Campanian ignimbrite. *Contrib. Mineral. Petrol.* **2014**, *167*, 1–18. [CrossRef]
60. Giaccio, B.; Hajdas, I.; Isaia, R.; Deino, A.; Nomade, S. High-precision $^{14}$C and $^{40}$Ar/$^{39}$Ar dating of the Campanian Ignimbrite (Y-5) reconciles the time-scales of climatic-cultural processes at 40 ka. *Sci. Rep.* **2017**, *7*, 45940. [CrossRef]
61. Deino, A.; Orsi, G.; de Vita, S.; Piochi, M. The age of the Neapolitan Yellow Tuff caldera-forming eruption (Campi Flegrei caldera Italy) assessed by $^{40}$Ar/$^{39}$Ar dating method. *J. Volcanol. Geotherm. Res.* **2004**, *133*, 157–170. [CrossRef]
62. Fedele, L.; Esposito, C.; Francios, L.; Morra, V.; Perrotta, A.; Santangelo, N.; Scarpati, C. Campi Flegrei e Procida. In *Guide Geologiche Reginonali_13 itinerari—Campania e Molise*; Calcaterra, D., D'Argenio, B., Ferranti, L., Pappone, G., Petrosino, P., Eds.; Società Geologica Italiana: Roma, Italy, 2016; pp. 69–84.
63. De Vivo, B.; Rolandi, G.; Gans, P.B.; Calvert, A.; Bohrson, W.A.; Spera, F.J.; Belkin, H.E. New constraints on the pyroclastic eruptive history of the Campanian volcanic plain (Italy). *Mineral. Petrol.* **2001**, *73*, 47–65. [CrossRef]
64. Rolandi, G.; Bellucci, F.; Heizler, M.; Belkin, H.E.; De Vivo, B. Tectonic controls on the genesis of ignimbrites from the Campanian Volcanic Zone, Southern Italy. *Mineral. Petrol.* **2003**, *79*, 3–31. [CrossRef]
65. Belkin, H.E.; Rolandi, G.; Jackson, J.C.; Cannatelli, C.; Doherty, A.L.; Petrosino, P.; De Vivo, B. Mineralogy and geochemistry of the older (> 40 ka) ignimbrites on the Campanian Plain, southern Italy. *J. Volcanol. Geotherm. Res.* **2016**, *323*, 1–18. [CrossRef]
66. Orsi, G.; de Vita, S.; Di Vito, M.A. The restless, resurgent Campi Flegrei nested caldera (Italy): Constraints on its evolution and configuration. *J. Volcanol. Geotherm. Res.* **1996**, *74*, 179–214. [CrossRef]
67. Pappalardo, L.; Civetta, L.; D'Antonio, M.; Deino, A.; Di Vito, M.; Orsi, G.; Carandente, A.; de Vita, S.; Isaia, R.; Piochi, M. Chemical and Sr- isotopical evolution of the Phlegrean magmatic system before the Campanian Ignimbrite and the Neapolitan Yellow Tuff eruptions. *J. Volcanol. Geotherm. Res.* **1999**, *91*, 141–166. [CrossRef]
68. Scarpati, C.; Sparice, D.; Perrotta, A. A crystal concentration method for calculating ignimbrite volume from distal ash-fall deposits and a reappraisal of the magnitude of the Campanian Ignimbrite. *J. Volcanol. Geotherm.* **2014**, *280*, 67–75. [CrossRef]
69. Fedele, L.; Scarpati, C.; Lanphere, M.; Melluso, L.; Morra, V.; Perrotta, A.; Ricci, G. The Breccia Museo formation, Campi Flegrei, southern Italy: Geochronology, chemostratigraphy and relationship with the Campanian Ignimbrite eruption. *Bull. Volcanol.* **2008**, *70*, 1189–1219. [CrossRef]
70. Fedele, L.; Scarpati, C.; Sparice, D.; Perrotta, A.; Laiena, F. A chemostratigraphic study of the Campanian Ignimbrite eruption (Campi Flegrei, Italy): Insights on magma chamber withdrawal and deposit accumulation as revealed by compositionally zoned stratigraphic and facies framework. *J. Volcanol. Geotherm. Res.* **2016**, *324*, 105–117. [CrossRef]
71. Silleni, A.; Giordano, G.; Isaia, R.; Ort, M.H. The Magnitude of the 39.8 ka Campanian Ignimbrite Eruption, Italy: Method, Uncertainties and Errors. *Front. Earth Sci.* **2020**, *8*, 543399. [CrossRef]
72. Pappalardo, L.; Ottolini, L.; Mastrolorenzo, G. The Campanian Ignimbrite (Southern Italy) geochemical zoning, insight on the generation of a super-eruption from catastrophic differentiation and fast withdrawal. *Contrib. Mineral. Petrol.* **2008**, *156*, 1–26. [CrossRef]
73. Scarpati, C.; Perrotta, A. Erosional characteristics and behaviour of large pyroclastic density currents. *Geology* **2012**, *40*, 1035–1038. [CrossRef]
74. Scarpati, C.; Perrotta, A. Stratigraphy and physical parameters of the Plinian phase of the Campanian Ignimbrite eruption. *Geol. Soc. Am. Bull.* **2016**, *128*, 1147–1159. [CrossRef]
75. Engwell, S.; Sparks, R.S.J.; Carey, S. Physical characteristics of tephra layers in the deep sea realm: The Campanian Ignimbrite eruption. *Geol. Soc. Spec. Publ.* **2014**, *398*, 47–64. [CrossRef]
76. Scarpati, C.; Sparice, D.; Perrotta, A. Facies variation in the Campanian Ignimbrite. *Rendiconti Online Soc. Geol. Ital.* **2015**, *33*, 83–87. [CrossRef]

77. Scarpati, C.; Sparice, D.; Perrotta, A. The ground layer of the Campanian Ignimbrite: An example of deposition from a dilute pyroclastic density current. *Bull. Volcanol.* **2015**, *77*, 97. [CrossRef]
78. Scarpati, C.; Sparice, D.; Perrotta, A. Comparative proximal features of the main Plinian deposits (Campanian Ignimbrite and Pomici di Base) of Campi Flegrei and Vesuvius. *J. Volcanol. Geotherm. Res.* **2016**, *321*, 149–157. [CrossRef]
79. Perrotta, A.; Scarpati, C. Volume partition between the plinian and co-ignimbrite air fall deposits of the Campanian Ignimbrite eruption. *Mineral. Petrol.* **2003**, *79*, 67–78. [CrossRef]
80. Pyle, D.M.; Ricketts, G.D.; Margari, V.; van Andel, T.H.; Sinitsyn, A.A.; Praslov, N.D.; Lisitsyn, S. Wide dispersal and deposition of distal tephra during the Pleistocene "Campanian Ignimbrite/Y5" eruption, Italy. *Quat. Sci. Rev.* **2006**, *25*, 2713–2728. [CrossRef]
81. Albert, P.G.; Giaccio, B.; Isaia, R.; Costa, A.; Niespolo, E.M.; Nomade, S.; Pereira, A.; Renne, P.R.; Hinchliffe, A.; Mark, D.F.; et al. Evidence for a large-magnitude eruption from Campi Flegrei caldera (Italy) at 29 ka. *Geology* **2019**, *47*, 595–599. [CrossRef]
82. Orsi, G.; D'Antonio, M.; de Vita, S.; Gallo, G. The Neapolitan Yellow Tuff, a large-magnitude trachytic phrcatoplinian eruption: Eruptive dynamics, magma withdrawtd and caldera collapse. *J. Volcanol. Geotherm. Res.* **1992**, *53*, 275–287. [CrossRef]
83. Orsi, G.; Civetta, L.; D'Antonio, M.; Di Girolamo, P.; Piochi, M. Step-filling and development of a three-layers magma chamber: The Neapolitan Yellow Tuff case history. *J. Volcanol. Geotherm. Res.* **1995**, *67*, 291–312. [CrossRef]
84. Scarpati, C.; Cole, P.; Perrotta, A. The Neapolitan Yellow Tuff—A large multiphase eruption from Campi Flegrei, Southem Italy. *Bull. Volcanol.* **1993**, *55*, 343–356. [CrossRef]
85. Smith, V.C.; Isaia, R.; Pearce, N.J.G. Tephrostratigraphy and glass compositions of post-15 ka Campi Flegrei eruptions: Implications for eruption history and chronostratigraphic markers. *Quat. Sci. Rev.* **2011**, *30*, 3638–3660. [CrossRef]
86. Di Vito, M.A.; Isaia, R.; Orsi, G.; Southon, J.; de Vita, S.; D'antonio, M.; Pappalardo, L.; Piochi, M. Volcanism and deformation in the past 12 ka at the Campi Flegrei caldera (Italy). *J. Volcanol. Geotherm. Res.* **1999**, *91*, 221–246. [CrossRef]
87. Cannatelli, C.; Lima, A.; Bodnar, R.J.; De Vivo, B.; Webster, J.D.; Fedele, L. Geochemistry of melt inclusions from the Fondo Riccio and Minopoli 1 eruptions at Campi Flegrei (Italy). *Chem. Geol.* **2007**, *237*, 418–432. [CrossRef]
88. Mangiacapra, A.; Moretti, R.; Rutherford, M.; Civetta, L.; Orsi, G.; Papale, P. The deep magmatic system of the Campi Flegrei caldera (Italy). *Geophys. Res. Lett.* **2008**, *35*, L21304. [CrossRef]
89. Forni, F.; Degruyter, W.; Bachmann, O.; De Astis, G.; Mollo, S. Long-term magmatic evolution reveals the beginning of a new caldera cycle at Campi Flegrei. *Sci. Adv.* **2018**, *4*, eaat940. [CrossRef]
90. Orsi, G.; Di Vito, M.A.; Isaia, R. Volcanic hazard assessment at the restless Campi Flegrei caldera. *Bull. Volcanol.* **2004**, *66*, 514–530. [CrossRef]
91. Tonarini, S.; D'Antonio, M.; DiVito, M.A.; Orsi, G.; Carandente, A. Geochemical and B-Sr-Nd isotopic evidence for mingling and mixing processes in the magmatic system that fed the Astroni volcano (4.1–3.8 ka) within the Campi Flegrei caldera (Southern Italy). *Lithos* **2009**, *107*, 135–151. [CrossRef]
92. Di Vito, M.A.; Arienzo, I.; Braia, G.; Civetta, L.; D'Antonio, M.; Di Renzo, V.; Orsi, G. The Averno 2 fissure eruption: A recent small-size explosive event at the Campi Flegrei Caldera (Italy). *Bull. Volcanol.* **2011**, *73*, 295–320. [CrossRef]
93. Mastrolorenzo, G. Averno Tuff ring in Campi Flegrei (South Italy). *Bull. Volcanol.* **1994**, *56*, 561–572. [CrossRef]
94. Arienzo, I.; Mazzeo, F.C.; Moretti, R.; Cavallo, A.; D'Antonio, M. Open-system magma evolution and fluid transfer at Campi Flegrei caldera (Southern Italy) during the past 5 ka as revealed by geochemical and isotopic data The example of the Nisida eruption. *Chem. Geol.* **2016**, *427*, 109–124. [CrossRef]
95. Piochi, M.; Mastrolorenzo, G.; Pappalardo, L. Magma ascent and eruptive processes fromtextural and compositional features of Monte Nuovo pyroclastic products, Campi Flegrei, Italy. *Bull. Volcanol.* **2005**, *67*, 663–678. [CrossRef]
96. Guidoboni, E.; Ciuccarelli, C. The Campi Flegrei caldera: Historical revision and new data on seismic crises, bradyseisms, the Monte Nuovo eruption and ensuing earthquakes (twelfth century 1582 ad). *Bull. Volcanol.* **2005**, *73*, 655–677. [CrossRef]
97. Liedl, A.; Buono, G.; Lanzafame, G.; Dabagov, S.B.; Della Ventura, G.; Hampai, D.; Mancini, L.; Marcelli, A.; Pappalardo, L. 3D imaging textural characterization of pyroclastic products from the 1538 AD Monte Nuovo eruption (Campi Flegrei, Italy). *Lithos* **2019**, *340*, 316–331. [CrossRef]
98. De Vita, S.; Orsi, G.; Civetta, L.; Carandente, A.; D'Antonio, M.; Deino, A.; di Cesare, T.; di Vito, M.A.; Fisher, R.V.; Isaia, R.; et al. The Agnano—Monte Spina eruption (4100 years BP) in the restless Campi Flegrei caldera (Italy). *J. Volcanol. Geotherm. Res.* **1999**, *91*, 269–301. [CrossRef]
99. Dellino, P.; Isaia, R.; La Volpe, L.; Orsi, G. Statistical analysis of textural data from complex pyroclastic sequences: Implications for fragmentation processes of the Agnano-Monte Spina Tephra (4.1 ka), Phlegraean Fields, Southern Italy. *Bull. Volcanol.* **2001**, *63*, 443–461.
100. Dellino, P.; Isaia, R.; La Volpe, L.; Orsi, G. Interaction between particles transported by fallout and surge in the deposits of the Agnano–Monte Spina eruption (Campi Flegrei Southern Italy). *J. Volcanol. Geotherm. Res.* **2004**, *133*, 193–210. [CrossRef]
101. Arienzo, I.; Moretti, R.; Civetta, L.; Orsi, G.; Papale, P. The feeding system of Agnano-Monte Spina eruption (Campi Flegrei, Italy): Dragging the past into the present activity and future scenarios. *Chem. Geol.* **2010**, *270*, 135–147. [CrossRef]
102. Romano, C.; Vona, A.; Campagnola, S.; Giordano, G.; Arienzo, I.; Isaia, R. Modelling and physico-chemical constraints to the 4.5 ka Agnano-Monte Spina Plinian eruption (Campi Flegrei, Italy). *Chem. Geol.* **2020**, *532*, 119301. [CrossRef]
103. Wu, W.N.; Schmitt, A.K.; Pappalardo, L. U-Th baddeleyite geochronology and its significance to date the emplacement of silica undersaturated magmas. *Am. Mineral.* **2015**, *10*, 2082–2090. [CrossRef]

104. Del Gaudio, C.; Aquino, I.; Ricciardi, G.P.; Ricco, C.; Scandone, R. Unrest episodes at Campi Flegrei: A reconstruction of vertical ground movements during 1905–2009. *J. Volcanol. Geotherm. Res.* **2010**, *195*, 48–56. [CrossRef]
105. Chiodini, G.; Caliro, S.; De Martino, P.; Avino, R.; Gherardi, F. Early signals of new volcanic unrest at Campi Flegrei caldera? Insights from geochemical data and physical simulations. *Geology* **2012**, *40*, 943–946. [CrossRef]
106. Chiodini, G.; Vandemeulebrouck, J.; Caliro, S.; D'Auria, L.; De Martino, P.; Mangiacapra, A.; Petrillo, Z. Evidence of thermal-driven processes triggering the 2005–2014 unrest at Campi Flegrei caldera. *Earth Planet. Sci. Lett.* **2015**, *414*, 58–67. [CrossRef]
107. Chiodini, G.; Paonita, A.; Aiuppa, A.; Costa, A.; Caliro, S.; De Martino, P.; Acocella, V.; Vandemeulebrouck, J. Magmas near the critical degassing pressure drive volcanic unrest towards a critical state. *Nat. Commun.* **2016**, *7*, 13712. [CrossRef] [PubMed]
108. Neri, A.; Bevilacqua, A.; Esposti Ongaro, T.; Isaia, R.; Aspinall, W.P.; Bisson, M.; Flandoli, F.; Baxter, P.J.; Bertagnini, A.; Iannuzzi, E.; et al. Quantifying volcanic hazard at Campi Flegrei caldera (Italy) with uncertainty assessment: II. Pyroclastic density current invasion maps. *J. Geophys. Res. Solid Earth* **2015**, *120*, 2309–2329. [CrossRef]
109. Charlton, D.; Kilburn, C.; Edwards, S. Volcanic unrest scenarios and impact assessment at Campi Flegrei caldera, Southern Italy. *J. Appl. Volcanol.* **2020**, *9*, 1–26. [CrossRef]
110. D'Antonio, M.; Civetta, L.; Di Girolamo, P. Mantle source heterogeneity in the Campanian region (South Italy) as inferred from geochemical and isotopic features of mafic volcanic rocks with shoshonitic affinity. *Mineral. Petrol.* **1999**, *67*, 163–192. [CrossRef]
111. Melluso, L.; de'Gennaro, R.; Fedele, L.; Franciosi, L.; Morra, V. Evidence of crystallization in residual, Cl–F-rich, agpaitic, trachyphonolitic magmas and primitive Mg-rich basalt–trachyphonolite interaction, in the lava domes of the Phlegrean Fields (Italy). *Geol. Mag.* **2012**, *149*, 532–550. [CrossRef]
112. Signorelli, S.; Vaggelli, G.; Francalanci, L.; Rosi, M. Origin of magmas feeding the Plinian phase of the Campanian Ignimbrite eruption, Phlegrean Fields (Italy): Constraints based on matrix-glass and glass-inclusion compositions. *J. Volcanol. Geotherm. Res.* **1999**, *91*, 199–220. [CrossRef]
113. Pappalardo, L.; Civetta, L.; de Vita, S.; Di Vito, M.; Orsi, G.; Carandente, A.; Fisher, R.V. Timing of magma extraction during the Campanian ignimbrite eruption (Campi Flegrei Caldera). *J. Volcanol. Geotherm. Res.* **2002**, *114*, 479–497. [CrossRef]
114. Webster, J.D.; Raia, F.; Tappen, C.; De Vivo, B. Pre-eruptive geochemistry of the ignimbrite-forming magmas of the Campanian Volcanic Zone, Southern Italy, determined from silicate melt inclusions. *Mineral. Petrol.* **2003**, *79*, 99–125. [CrossRef]
115. Munno, R.; Petrosino, P. New constraints on the occurrence of Y-3 upper Pleistocene tephra marker layer in the tyrrhenian sea. *Il Quaternario* **2004**, *17*, 11–20.
116. D'Oriano, C.; Poggianti, E.; Bertagnini, A.; Cioni, R.; Landi, P.; Polacci, M.; Rosi, M. Changes in eruptive style during the A.D. 1538 Monte Nuovo eruption (Phlegrean Fields, Italy): The role of syn-eruptive crystallization. *Bull. Volcanol.* **2005**, *67*, 601–621. [CrossRef]
117. Marianelli, P.; Sbrana, A.; Proto, M. Magma chamber of the Campi Flegrei supervolcano at the time of eruption of the Campanian Ignimbrite. *Geology* **2006**, *34*, 937–940. [CrossRef]
118. Fowler, S.J.; Spera, F.J.; Bohrson, W.A.; Belkin, H.E.; De Vivo, B. Phase Equilibria Constraints on the Chemical and Physical Evolution of the Campanian Ignimbrite. *J. Petrol.* **2007**, *48*, 459–493. [CrossRef]
119. Fedele, L.; Zanetti, A.; Morra, V.; Lustrino, M.; Melluso, L.; Vannucci, R. Clinopyroxene/liquid trace element partitioning in natural trachyte–trachyphonolite systems: Insights from Campi Flegrei (Southern Italy). *Contrib. Mineral. Petrol.* **2009**, *158*, 337–356. [CrossRef]
120. Arienzo, I.; Neumann, A.; Wörner, G.; Civetta, L.; Orsi, G. Processes and timescales of magma evolution prior to the Campanian ignimbrite eruption (Campi Flegrei, Italy). *Earth Planet. Sci. Lett.* **2011**, *306*, 217–228. [CrossRef]
121. Fourmentraux, C.; Métrich, N.; Bertagnini, A.; Rosi, M. Crystal fractionation, magma step ascent, and syn-eruptive mingling: The Averno 2 eruption (Phlegraean Fields, Italy). *Contrib. Mineral. Petrol.* **2012**, *163*, 1121–1137. [CrossRef]
122. Tomlinson, E.L.; Arienzo, I.; Civetta, L.; Wulf, S.; Smith, V.C.; Hardiman, M.; Lane, C.S.; Carandente, A.; Orsi, G.; Rosi, M.; et al. Geochemistry of the Phlegraean Fields (Italy) proximal sources for major Mediterranean tephras: Implications for the dispersal of Plinian and coignimbritic components of explosive eruptions. *Geochim. Cosmochim. Acta* **2012**, *93*, 102–128. [CrossRef]
123. Roeder, P.L.; Emslie, R. Olivine-liquid equilibrium. *Contrib. Mineral. Petrol.* **1970**, *29*, 275–289. [CrossRef]
124. Matzen, A.K.; Baker, M.B.; Beckett, J.R.; Stolper, E.M. Fe–Mg partitioning between olivine and high-magnesian melts and the nature of Hawaiian parental liquids. *J. Petrol.* **2011**, *52*, 1243–1263. [CrossRef]
125. Grove, T.L.; Bryan, W.B. Fractionation of pyroxene-phyric MORB at low pressure: And experimental study. *Contrib. Mineral. Petrol.* **1983**, *84*, 293–309. [CrossRef]
126. Mollo, S.; Putirka, K.; Misiti, V.; Soligo, M.; Scarlato, P. A new test for equilibrium based on clinopyroxene-melt pairs: Clues on the solidification temperatures of Etnean alkaline melts on clinopyroxene- melt pairs: Clues on the solidification temperatures of Etnean alkaline melts at post-eruptive conditions. *Chem. Geol.* **2013**, *352*, 92–100. [CrossRef]
127. Putirka, K.D. Clinopyroxene + liquid equilibria to 100 kbar and 2450 K. *Contrib. Mineral. Petrol.* **1999**, *135*, 151–163. [CrossRef]
128. Mollo, S.; Masotta, M.; Forni, F.; Bachmann, O.; De Astis, G.; Moore, G.; Scarlato, P. A K-feldspar-liquid hygrometer specific to alkaline differentiated magmas. *Chem. Geol.* **2015**, *392*, 1–8. [CrossRef]
129. Putirka, K.; Perfit, M.; Ryerson, F.J.; Jackson, M.G. Ambient and excess mantle temperatures, olivine thermometry, and active vs. passive upwelling. *Chem. Geol.* **2007**, *241*, 177–206. [CrossRef]
130. De Hoog, J.C.; Gall Cornell, L.D.H. Trace-element geochemistry of mantle olivine and application to mantle petrogenesis and geothermobarometry. *Chem. Geol.* **2010**, *270*, 196–215. [CrossRef]

131. Kahl, M.; Chakraborty, S.; Pompilio, M.; Costa, F. Constraints on the nature and evolution of the magma plumbing system of Mt Etna volcano (1991–2008) from a combined thermodynamic and kinetic modelling of the compositional record of minerals. *J. Petrol.* **2015**, *56*, 2025–2068. [CrossRef]
132. Moretti, R.; Arienzo, I.; Orsi, G.; Civetta, L.; D'Antonio, M. The deep plumbing system of Ischia: A physico-chemical window on the fluid-saturated and $CO^2$-sustained Neapolitan volcanism (Southern Italy). *J. Petrol.* **2013**, *54*, 951–984. [CrossRef]
133. Di Salvo, S.; Avanzinelli, R.; Isaia, R.; Zanetti, A.; Druitt, T.; Francalanci, L. Crystal-mush reactivation by magma recharge: Evidence from the Campanian Ignimbrite activity, Campi Flegrei volcanic field, Italy. *Lithos* **2020**, *376–377*, 105780. [CrossRef]
134. D'Antonio, M.; Tonarini, S.; Arienzo, I.; Civetta, L.; Di Renzo, V. Components and processes in the magma genesis of the Phlegrean Volcanic District, Southern Italy. *Geol. Soc. Am.* **2007**, *418*, 203–220.
135. Pappalardo, L.; Mastrolorenzo, G. Rapid differentiation in a sill-like magma reservoir: A case study from the campi flegrei caldera. *Sci. Rep.* **2012**, *2*, 712. [CrossRef]
136. Rhodes, J.M.; Lofgren, G.E.; Smith, D.P. One atmosphere melting experiments on ilmenite basalt 12008. *Proc. Lunar Planet. Sci. Conf.* **1979**, *5*, 407–422.
137. Mollo, S.; Del Gaudio, P.; Ventura, G.; Iezzi, G.; Scarlato, P. Dependence of clinopyroxene composition on cooling rate in basaltic magmas: Implications for thermobarometry. *Lithos* **2010**, *118*, 302–312. [CrossRef]
138. Gee, L.L.; Sack, R.O. Experimental petrology of melilite nephelinites. *J. Petrol.* **1988**, *29*, 1235–1255. [CrossRef]
139. Costa, F.; Chakraborty, S. Decadal time gaps between mafic intrusion and silicic eruption obtained from chemical zoning patterns in olivine. *Earth Planet. Sci. Lett.* **2004**, *227*, 517–530. [CrossRef]
140. Costa, F.; Dohmen, R.; Chakraborty, S. Time scales of magmatic processes from modeling zoning patterns of crystals. *Rev. Mineral. Geochem.* **2008**, *69*, 545–594. [CrossRef]
141. Costa, F.; Morgan, D. Time constraints from chemical equilibration in magmatic crystals. In *Timescales of Magmatic Processes: From Core to Atmosphere*; Dosseto, A., Turner, S., Van-Orman, J., Eds.; Wiley: Chichester, UK, 2011; pp. 125–159.
142. Petrone, C.; Bugatti, G.; Braschi, E.; Tommasini, S. Pre-eruptive magmatic processes re-timed using a non-isothermal approach to magma chamber dynamics. *Nat. Comm.* **2016**, *7*, 12946. [CrossRef]
143. Dohmen, R.; Faak, K.; Blundy, J.D. Chronometry and speedometry of magmatic processes using chemical diffusion in olivine, plagioclase and pyroxenes. *Rev. Mineral. Geochem.* **2017**, *83*, 535–575. [CrossRef]
144. Chakraborty, S. Diffusion in silicates: A tool to track timescales of processes comes of age. *Annu. Rev. Earth Planet. Sci.* **2008**, *36*, 153–190. [CrossRef]
145. Armienti, P.; Barberi, F.; Bizouard, H.; Clocchiatti, R.; Innocenti, F.; Metrich, N.; Rosi, M.; Sbrana, A. The Phlegraean Fields: Magma evolution within a shallow chamber. *J. Volcanol. Geotherm. Res.* **1983**, *17*, 289–311. [CrossRef]
146. Fuhrman, M.L.; Lindsley, D.H. Ternary-feldspar modeling and thermometry. *Am. Min.* **1988**, *73*, 201–215.
147. Edmonds, M. New geochemical insights into volcanic degassing. *Philos. Trans. R. Soc. A Math. Phys. Eng. Sci.* **2008**, *366*, 4559–4579. [CrossRef]
148. Sigmundsson, F.; Hreinsdottir, S.; Hooper, A.; Arnadottir, T.; Pedersen, R.; Roberts, J.M.; Oskarsson, N.; Auriac, A.; Decriem, J.; Einarsson, P.; et al. Intrusion triggering of the 2010 Eyjafjallajokull explosive eruption. *Nature* **2010**, *468*, 426–430. [CrossRef]
149. Tarasewicz, J.; White, R.S.; Brandsdottir, B.; Schoonman, C.M. Seismogenic magma intrusion before the 2010 eruption of Eyjafjallajokull volcano, Iceland. *Geophys. J. Int.* **2014**, *198*, 906–921. [CrossRef]
150. Henstock, T.J.; Woods, A.W.; White, R.S. The accretion of oceanic crust by episodic sill intrusion. *J. Geophys. Res.* **1993**, *98*, 4143–4161. [CrossRef]
151. Kelemen, P.B.; Koga, K.T.; Shimizu, N. Geochemistry of gabbro sills in the crust-mantle transition zone of the Oman ophiolite: Implications for the origin of the oceanic lower crust. *Earth Planet. Sci. Lett.* **1997**, *146*, 475–488. [CrossRef]
152. Annen, C.; Blundy, J.D.; Sparks, R.S.J. The genesis of intermediate and silicic magmas in deep crustal hot zones. *J. Petrol.* **2006**, *47*, 505–539. [CrossRef]
153. Bianchi, R.; Coradini, A.; Federico, C.; Giberti, G.; Luciano, P.; Pozzi, J.P.; Sartoris, G.; Scandone, R. Modelling of surface ground deformation in volcanic areas: The 1970–1972 and 1982–1984 crises of Campi Flegrei, Italy. *J. Geophys. Res.* **1987**, *92*, 139–150.
154. Ferrucci, F.; Him, A.; De Natale, G.; Virieux, J.; Mirabile, L. P-SV convertions at a shallow boundary beneath Campi Flegrei caldera (Italy): Evidence for the magma chamber. *J. Geophys. Res.* **1992**, *97*, 351–359.
155. De Gori, P.; Cimini, G.B.; Chiarabba, C.; De Natale, G.; Troise, C.; Deschamps, A. Teleseismic tomography of the Campanian volcanic area and surrounding Apenninic belt. *J. Volcanol. Geotherm. Res.* **2001**, *109*, 52–75. [CrossRef]
156. Chiarabba, C.; Moretti, M. An insight into the unrest phenomena at the Campi Flegrei caldera from Vp and Vp/Vs tomography. *Terra Nova* **2006**, *18*, 373–379. [CrossRef]
157. Guidarelli, M.; Saraò, A.; Panza, G.F. Surface wave tomography and seismic source studies at Campi Flegrei (Italy). *Phys. Earth Planet. Inter.* **2002**, *134*, 157–173. [CrossRef]
158. De Vivo, B.; Petrosino, P.; Lima, A.; Rolandi, G.; Belkin, H.E. Research progress in volcanology in the Neapolitan area, southern Italy: A review and some alternative views. *Miner. Petrol.* **2010**, *99*, 1–28. [CrossRef]
159. Vetere, F.; Holtz, F.; Behrens, H.; Botcharnikov, R.E.; Fanara, S. The effect of alkalis and polymerization on the solubility of $H_2O$ and $CO_2$ in alkali-rich silicate melts. *Contrib. Mineral. Petrol.* **2014**, *202*, 251–261. [CrossRef]
160. Capuano, P.; Russo, G.; Civetta, L.; Orsi, G.; D'Antonio, M.; Moretti, R. The active portion of the Campi Flegrei caldera structure imaged by 3-D inversion of gravity data. *Geochem. Geophys.* **2013**, *14*, 4681–4697. [CrossRef]

161. Carlino, S.; Kilburn, C.R.J.; Tramelli, A.; Troise, C.; Somma, R.; De Natale, G. Tectonic stress and renewed uplift at Campi Flegrei caldera, Southern Italy: New insights from caldera drilling. *Earth Planet. Sci. Lett.* **2015**, *420*, 23–29. [CrossRef]
162. Voloschina, M.; Pistolesi, M.; Bertagnini, A.; Métrich, N.; Pompilio, M.; Di Roberto, A.; Di Salvo, S.; Francalanci, L.; Isaia, R.; Cioni, R.; et al. Magmatic reactivation of the Campi Flegrei volcanic system: Insights from the Baia–Fondi di Baia eruption. *Bull. Volcanol.* **2018**, *80*, 75. [CrossRef]
163. Stock, M.J.; Humphreys, M.C.S.; Smith, V.C.; Isaia, R.; Brooker, R.A.; Pyle, D.M. Tracking volatile behaviour in sub-volcanic plumbing systems using apatite and glass: Insights into pre-eruptive processes at Campi Flegrei, Italy. *J. Petrol.* **2018**, *59*, 2463–2492. [CrossRef]
164. Bohrson, W.A.; Spera, F.J.; Fowler, S.J.; Belkin, H.E.; DeVivo, B. Petrogenesis of the Campanian Ignimbrite: Implications for crystal–melt separation and open-system processes from major and trace elements and Th isotope data. In Volcanism in the Campania Plain, Vesuvius, Campi Flegrei and Ignimbrites. *Dev. Volcanol.* **2006**, *9*, 249–288.
165. Moretti, R.; Arienzo, I.; Di Renzo, V.; Orsi, G.; Arzilli, F.; Brune, F.; D'Antonio, M.; Mancini, L.; Deloule, E. Volatile segregation and generation of highly vesiculated explosive magmas by volatile-melt fining processes: The case of the Campanian Ignimbrite eruption. *Chem. Geol.* **2019**, *503*, 1–14. [CrossRef]
166. Berrino, G.; Corrado, G.; Riccardi, U. Sea gravity data in the Gulf of Naples. A contribution to delineating the structural pattern of the Phlegraean Volcanic District. *J. Volcanol. Geotherm. Res.* **2008**, *175*, 241–252. [CrossRef]
167. Ruth, D.C.S.; Costa, F.; Bouvet de Maisonneuve, C.; Franco, L.; Cortés, J.A.; Calder, E.S. Crystal and melt inclusion timescales reveal the evolution of magma migration before eruption. *Nat. Commun.* **2018**, *9*, 2657. [CrossRef]